

Two Types of Granites in the Western Yangtze Block and Their Implications for Regional Tectonic Evolution: Constraints from Geochemistry and Isotopic Data

MABI Awei¹, YANG Zhengxi^{1,*}, ZHANG Mingchun², WEN Dengkui²,
LI Yanlong² and LIU Xuyang³

1 School of Earth Sciences, Chengdu University of Technology, Chengdu 610059, Sichuan, China

2 Panxi Team, Sichuan Bureau of Geology and Mineral Resources, Xichang 615000, Sichuan, China

3 Department of Geological Sciences, The University of Texas at El Paso, El Paso 79968, Texas, USA

Abstract: In the western Yangtze Block, widespread Mesoproterozoic to Neoproterozoic rocks are the key to understanding the Precambrian tectonic-magmatic evolution of the region. However, their petrogenesis and tectonic setting are still controversial. In this paper, zircon U-Pb ages, Sm-Nd isotopic and whole-rock geochemical data are reported from selected fresh samples in the southern Dechang county, southwestern China, in order to constrain their emplacement age and magma source, as well as their petrogenesis and tectonic setting. They are mainly composed of biotite monzogranite, monzonitic granite, biotite granodiorites, and quartz diorite. Two ages of 1055 ± 43 Ma and 837.6 ± 3.8 Ma were obtained through zircon U-Pb dating by LA-ICP-MS and LA-MC-ICP-MS, respectively. According to their major element compositions, the Grenville-age granites are peraluminous calc-alkaline series calcic S-type granite. In contrast, the mid-Neoproterozoic granites are metaluminous calc-alkaline series alkalic I-type granite. Furthermore, the S-type granites are enriched in LREEs relative to HREEs with $(\text{La}/\text{Yb})_{\text{N}}$ ratios of 3.85–18.56 and underwent major fractionation with strongly negative Eu anomalies ($\text{Eu}/\text{Eu}^* = 0.38\text{--}0.66$). In the MORB-normalized trace element variation diagram, all the samples are enriched in Ce and large ion lithophile elements such as Rb, Th, and K, and depleted in high field strength elements such as Nb, and Ti, with negative Sr and Ti anomalies. The I-type granites are enriched in LREEs with slight negative Eu anomalies ($\text{Eu}/\text{Eu}^* = 0.83\text{--}0.93$). They are characterized by the enrichment of highly incompatible elements (such as K, Rb, Ba, Th) and LREEs, relative to MORB. Neodymium isotopic data show that the S-type granites display $^{143}\text{Nd}/^{144}\text{Nd}$ values of 0.51241–0.51256, and have ε_{Nd} ($t = 1055$ Ma) values of (-3.29) to (-3.81) . Calculated t_{DM} ages yield values from 1.87 to 1.91 Ga with the $t_{\text{DM-2stg}}$ ages of 1.86 to 1.9 Ga. The I-type granites have $^{143}\text{Nd}/^{144}\text{Nd}$ ratios between 0.51192 and 0.51195, corresponding to initial ε_{Nd} ($t = 837$ Ma) values of 1.22 to 5.63. Calculated t_{DM} ages yield values from 1.0 to 1.38 Ga and the $t_{\text{DM-2stg}}$ ages yield values from 0.99 to 1.06 Ga. The S-type granites are distinguished as syn-collision granite, whereas the I-type granites were formed as arc magmas according to the Rb-(Yb+Ta) and R_1 - R_2 tectonic discrimination diagrams. To conclude, there are two types of spatially associated granite, the Mesoproterozoic S-type granite which were derived from remelting of upper crustal mudstone and/or clastics and resulted from the convergence of two continental plates, and the mid-Neoproterozoic I-type granite which formed in continental arc and resulted from mantle-derived magma mixed crust material, in the western Yangtze Block. Furthermore, we suggest that collision between the Yangtze and Cathaysia blocks occurred at about 1055 Ma, and caused the S-type granite. The I-type granite related to the subduction of oceanic lithosphere eastward underneath the Yangtze Block in the mid-Neoproterozoic.

Key word: I-type granite, S-type granite, geochemistry, petrogenesis, tectonic setting, Western Yangtze Block

* Corresponding author. E-mail: yzx@cduet.edu.cn

1 Introduction

The South China Craton is one of the major tectonic terranes in China, which consists of the Yangtze Block in the northwest and the Cathaysia Block in the southeast (Zhang Heng et al., 2015; Sun Ya et al., 2016). The Yangtze Block, which is presently surrounded by the Eurasia Plate to the north, India Plate to the west and the Pacific Ocean Plate to the east, is an important area to understanding the geological evolution of the Craton.

Mesoproterozoic to Neoproterozoic rocks are widely exposed along the margins of the Yangtze Block including volcanic-sedimentary strata, Grenville-age granites and Neoproterozoic felsic rocks associated with mafic intrusions (Geng Yuansheng et al., 2008; Zhao, 2008; Zhao, 2010; Chen, 2013). These widespread Precambrian rocks are the key to studying the Precambrian tectonic evolution of the Yangtze Block. However, their petrogenesis and tectonic setting, and the Precambrian tectonic-magmatism evolution of the Yangtze Block remain to be answered.

It is generally accepted that the South China Craton was formed through the amalgamation of the Yangtze and Cathaysia blocks along the Sibao/Jiangnan Orogeny. However, the timing of final assembly of these two blocks is still controversial (Chen et al., 2014; Li Zuochen et al., 2015; Wang et al., 2015; Zhao, 2015; Wu et al., 2016; Chen et al., 2016). One school of thought has suggested that Sibao/Jiangnan Orogeny was part of the global Grenvillian Orogeny and place the South China Craton between Australia-East Antarctica and Laurentia in Rodinia as “missing-link” model (Li et al., 1995; Li et al., 2002; Pisarevsky et al., 2003; Greentree et al., 2006; Li et al., 2007b; Li et al., 2008). Furthermore, they urged that widespread Neoproterozoic magmatism was related to the breakup of supercontinent Rodinia (Li et al., 1995; Li et al., 2002; Li et al., 2006, 2007a; Li et al., 2008; Cui et al., 2015). Whereas, the other school places the South China Craton on the NW margin of supercontinent Rodinia rather than within it (Zhou et al., 2006). They proposed that Sibao/Jiangnan Orogeny formed at Neoproterozoic and lasted until ca. 800 Ma or even later, and a long-lived oceanic subduction lasted until ca. 730 Ma in the side of western margin of Yangtze Block (Zhou et al., 2002; Chen, 2013; Wang et al., 2015; and references therein). They suggested that Neoproterozoic intrusions formed in a continental arc related to the steeply dipping subduction of oceanic lithosphere eastwards underneath the active continental margin of Yangtze Block (Zhou et al., 2002; Zhou et al., 2006; Zhou et al., 2007; Zhao, 2008; Sun, 2009; Zhao, 2010). In addition, other authors proposed that these Neoproterozoic rocks resulted from a rift event

related to post-collisional relaxation (Zheng et al., 2007; Zheng et al., 2008), as well as a long-lived oceanic subduction caused by back-arc spreading (Zhao et al., 2011). Recently, Zhao (2015) proposed a “divergent double-sided subduction” model for the Jiangnan/Sibao Orogen which eventually led to the soft collision of Yangtze and Cathaysia blocks at ca. 825 Ma.

In this paper, we present geochemical and isotopic data for the two types of spatially associated granites from the western Yangtze Block, with the aim of constraining their age, petrogenesis, tectonic setting, and their significance in the Precambrian tectonic-magmatic evolution of the western Yangtze Block.

2 Geological Background

The western Yangtze Block, which is traditionally called “Kangdian Geaxis”, is separated from the Songpan-Ganzi Block by the Jinhe fault in the west and Sichuan Basin by the Xiaojiang fault in the east. It is a N-S-trending tectonic belt approximately 700 km in length, 50 km–100 km in width (Geng Yuansheng et al., 2008) (Fig. 1).

The oldest rocks known in this belt form the Dahongshan Group, in which the meta-volcanic unit yielded a SHRIMP zircon U-Pb age of 1675 ± 8 Ma (Greentree and Li, 2008; Zhao, 2010). The Dahongshan Group mainly crops out in Yunnan province and is comprised of a sequence of meta-volcanic-sedimentary rocks of lower amphibolite facies metamorphism, with meta-conglomerate, carbonate, amphibolite, quartzite, and mica schist. However, the formation and evolution processes of its sedimentary basin and associated igneous rocks are poorly understood (Zhao, 2010; Chen, 2013; and references therein). The Dahongshan Group was considered to be unconformably overlain by the Kunyang Group. In Sichuan province, in our study region, the Huili Group was considered to be the equivalent strata of the Kunyang Group (Zhao, 2010 and references therein; Li Bo et al., 2016). These rocks are commonly deformed or locally metamorphosed under lower greenschist facies conditions (Chen, 2013; and references therein). In addition, the Mesoproterozoic Grenvillian-age intrusions are rare, and sporadically distributed.

Neoproterozoic strata are also distributed in the margin of Yangtze Block. In parts of Sichuan, Neoproterozoic volcanic-sedimentary sequences are known as the Yanbian, and Suxiong groups and are in fault contact with the Huili Group. They consist of volcanic assemblages and a thick flysch sequence, and detrital zircon dating constrains the deposition ages range between 900 and 800 Ma (Zhao, 2008; Zhao, 2010; Chen, 2013; and references therein).

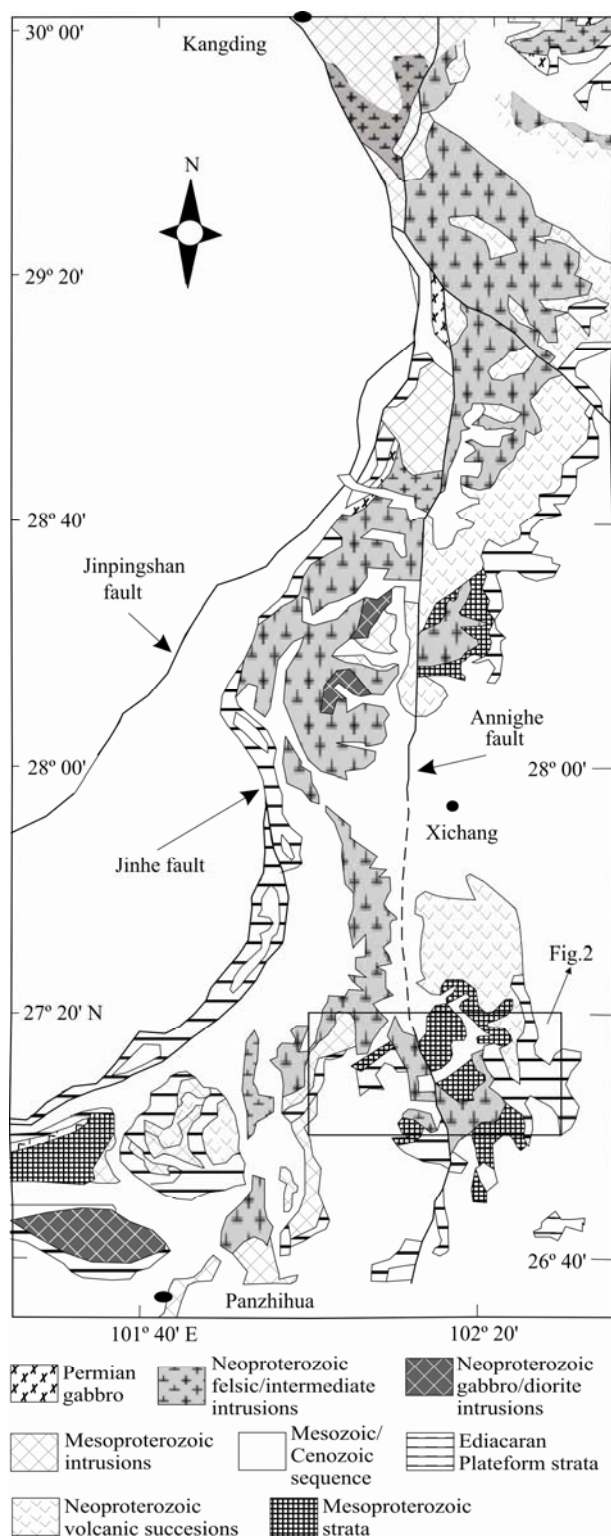


Fig. 1. A simplified geological map of the western margin of Yangtze Block, south western China (modified after Huang et al., 2009).

The Neoproterozoic intrusions in the periphery of Yangtze Block are characterized by predominant felsic and minor mafic-ultramafic intrusions (Chen et al., 2015), which consist mainly of TTG gneisses, granites, diorites

and gabbros (Chen et al., 2016). Furthermore, the available zircon U-Pb ages on these plutons range from 860 to 740 Ma (Zhou et al., 2002; Zhou et al., 2006; Munteanu and Yao, 2007; Zhao, 2008; Pei Xianzhi et al., 2009; Zhao, 2010; Dong et al., 2011; Dong et al., 2012; Chen, 2013; and references therein).

The samples for our study were collected from complexes named the “Jinchuan-Mosuoying” complex and “Mopan Mountain-Cida” complex in previous studies. The “Jinchuan-Mosuoying” complex is exposed from the northern Huili county to the southern Dechang county, about 35 km long, and is unconformably covered by the lower Sinian Lieguliu Formation (Z_1l). It also intrudes the Huili Group. The “Mopan Mountain-Cida” complex is exposed from Xichang to the north and Dechang county to the south and intruded the Neoproterozoic rocks or/and mostly are in fault contact with the country rock.

3 Analytical Methods

3.1 Major and trace element analyses

Whole-rock major and trace element data were obtained at the SW Metallurgical Geological Mineral Testing Center, China. The rock samples were powdered in an agate mortar. Major elements were determined by X-ray fluorescence spectrometry (XRF; PW4400/40). Fused glass disks were analyzed and the analytical precision, as determined on the Chinese National Standard GSR-1 and GSR-3, was better than 5%. Loss on ignition (LOI) was obtained using 1 g powder heated up to 1100°C for 1 h. Trace elements including REE were determined by Inductively Coupled Plasma Mass Spectrometer (ICP-MS; XSERIES II) with RSD < 2–10%. The in-run analytical precision for most trace elements was better than 5%.

3.2 U–Pb zircon analysis

The zircon grains were separated using conventional heavy liquid and magnetic techniques, and the representative zircons were hand-picked under a binocular microscope. The zircons were mounted in epoxy, polished, coated with gold, and photographed in transmitted and reflected light to identify grains for analysis. Cathodoluminescence (CL) images were taken using a Quanta 450 FEG electron microscope.

For samples D3034 and D3070, The U-Pb isotopic ratios of zircon separates were measured using the LA-ICP-MS at State Key Laboratory of Geological Processes and Mineral Resources, China University of Geosciences, Wuhan. The GeoLas 2500 laser-ablation system equipped with a 193 nm ArF excimer laser (LA) and Agilent7500a (ICP-MS) were used to determine the zircon U–Pb ages at a spot diameter of 24 μm –32 μm . For methods, refer to Qi

et al. (2014).

For sample D3202, Zircon U–Pb analysis was carried out at the Tianjin Center, China Geological Survey, using laser ablation-multicollector inductively coupled-plasma mass spectrometry (LA–MC–ICP–MS) and a Thermo Fisher Scientific Neptune instrument with an ESI UP193-FX ArF excimer laser. The laser wave-length is 193 nm and a pulse rate of ~ 5 ns was used during analysis. The very short wavelength has been demonstrated to yield superior control in particle size distribution, thereby greatly enhancing vaporization, atomization, and ionization within the ICP. The spot size is adjustable (25 μm –150 μm) and laser pulse frequency of 1 Hz–200 Hz. Based on the reflected and transmitted light photomicrographs and cathodoluminescence (CL) images, the laser was focused on producing ablation pits ranging in diameter from 35 μm to 50 μm , using a laser pulse rate of 8 Hz–10 Hz with an energy density of approximately 13 J/cm²–14 J/cm², and using He as the carrier gas. The standard zircons 91500 and GJ-1 were used for calibrating the raw data. The details of the analytical procedures have been described by Yuan et al. (2011) and Yang et al. (2014).

3.3 Sm–Nd isotopic analysis

The samples were spiked with a mixed ¹⁴⁵Nd–¹⁴⁹Sm spike, prior to dissolution, and were dissolved in Teflon breakers for >72 hours using a mixture of acids (HF + HNO₃). Two-column ion exchange techniques were

employed to separate Sm and Nd. Isotopic measurements were performed on a Finnigan MAT-262 thermal ionization mass spectrometer (TIMS) at the Isotopic Geochemistry Laboratory of Yichang Institute of Geology and Mineral Resources. Procedural blanks were <200 pg for Sm and Nd. ¹⁴³Nd/¹⁴⁴Nd ratios were corrected for instrumental mass fractionation with ¹⁴⁶Nd/¹⁴⁴Nd = 0.7219 and normalized to La Jolla standard value of 0.511863 \pm 8 (2 sigma).

4 Petrography

Two types of granite, the Mesoproterozoic S-type granite (group B) and the Neoproterozoic I-type granite (group A), were distinguished in this study. The detailed geological mapping was conducted, and six biotite monzogranites (D3033, D3034, D3070, D3092, D3220, D3227), two monzonitic granites (D3053, D3056), one biotite granodiorite (D3094) from S-type granite, as well as four biotite monzogranites (D3050, D3052, D3067, D3204) and two quartz diorites (D3069, D3202) from I-type granite were collected (Fig. 2). The petrography of the two types of granite is listed in Table 1, and representative field photographs are shown in Fig. 3.

5 Analytical Results

5.1 Major elements

Major oxide compositions of the samples are listed in

Table 1 Results of the petrographic characterization of the granitoids in this study

Igneous classification	Lithology	Texture	Structure	Modal mineral (%)						
				Q	Kfs	Pl	Bt	Ms	Am	Accessory mineral
I-type granite	Quartz diorite	Granular texture	Massive structure	5–15	0–2	50–57	5–20		5–35	1–3
	Biotite monzogranite	Medium- to coarse-grained granitic texture	Massive structure	53	25	20	2			rare
	Biotite granodiorites	Porphyaceous texture	Massive structure	30–32	10–15	43–46	10–13			rare
S-type granite	Monzonitic granite	Porphyaceous texture	Massive structure	45	28	27				
	Biotite monzogranite	Porphyaceous texture	Massive structure	30–35	10–35	30–47	5–15	0–3		

Table 2 Major element (%) compositions for two types of Granite in the western Yangtze Block

	S-type granite										I-type granite					
	D3033	D3034	D3053	D3056	D3070	D3092	D3094	D3220	D3227	D3050	D3052	D3067	D3069	D3202	D3204	
SiO ₂	75.14	68.14	71.19	70.72	73.56	69.89	69.55	75.62	76.42	49.71	49.47	45.04	48.38	52.08	50.48	
Al ₂ O ₃	13.84	15.34	14.02	14.48	12.97	14.95	14.75	13.34	12.41	14.87	19.68	14.96	12.85	14.17	15.79	
Fe ₂ O ₃	1.06	0.735	0.51	0.62	1.47	0.91	0.19	0.66	0.55	2.2	5.08	2.44	2.1	2.71	1.73	
FeO	0.09	4.38	3.34	2.86	1.3	2.67	3.97	0.65	1.55	7.64	5.16	12.6	12.6	7.04	8.5	
CaO	0.36	1.28	1.11	1.16	0.63	0.54	1.18	0.19	0.44	8.96	9.12	9.53	9.8	8.33	8.24	
MgO	0.11	1.16	0.74	0.75	0.50	0.97	0.88	0.30	0.83	6.88	4.73	7.55	5.33	5.7	5.92	
K ₂ O	5.52	4	4.71	4.53	4.99	4.54	4.21	6.2	1.97	1.98	0.33	0.54	0.55	1.86	2.03	
Na ₂ O	2.73	1.4	1.48	2.34	2.24	1.99	2.13	0.72	3.5	2.94	3.48	2.1	2.47	3.41	2.31	
TiO ₂	0.05	0.70	0.49	0.49	0.41	0.49	0.62	0.18	0.32	1.45	1.07	2.1	2.83	1.49	1.49	
P ₂ O ₅	0.14	0.18	0.15	0.17	0.19	0.23	0.23	0.13	0.16	0.32	0.29	0.22	0.44	0.40	0.33	
MnO	0.01	0.08	0.04	0.03	0.03	0.04	0.06	0.02	0.02	0.16	0.16	0.21	0.27	0.17	0.18	
Lol	0.69	2.23	1.79	1.45	1.45	2.42	1.87	1.68	1.62	2.4	1.06	2.16	1.98	2.22	2.6	
H ₂ O ⁺	0.50	1.53	1.18	1.02	1.28	2.08	1.31	1.34	1.19	1.46	0.75	1.12	1.21	1.55	2.02	
CO ₂	0.08	0.08	0.07	0.09	0.05	0.11	0.06	0.08	0.15	0.22	0.11	0.10	0.49	0.09	0.14	

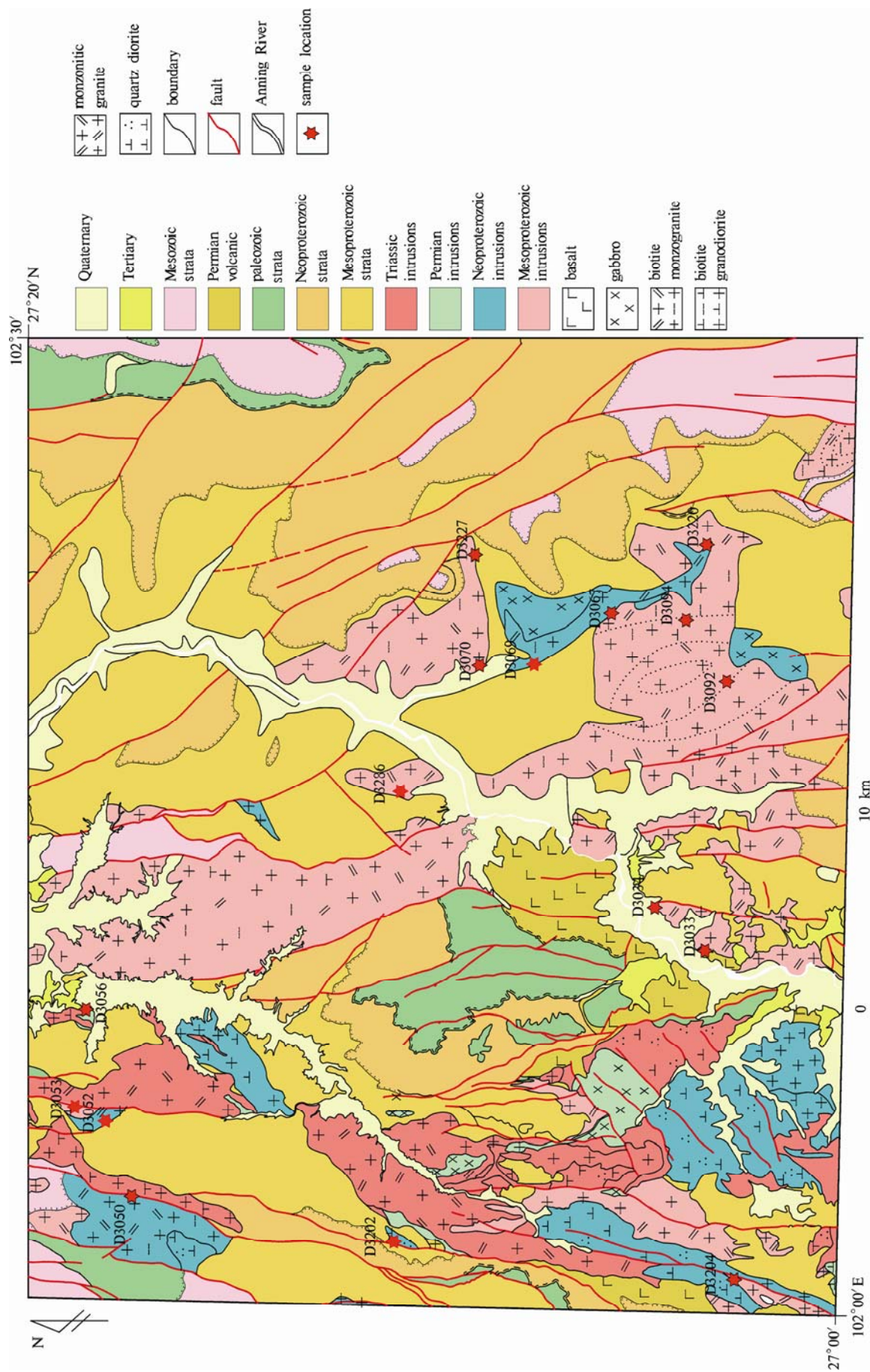


Fig. 2. The Geological map of Dechang region, Sichuan province, SW China, showing the sampling locations as dots and numbers.

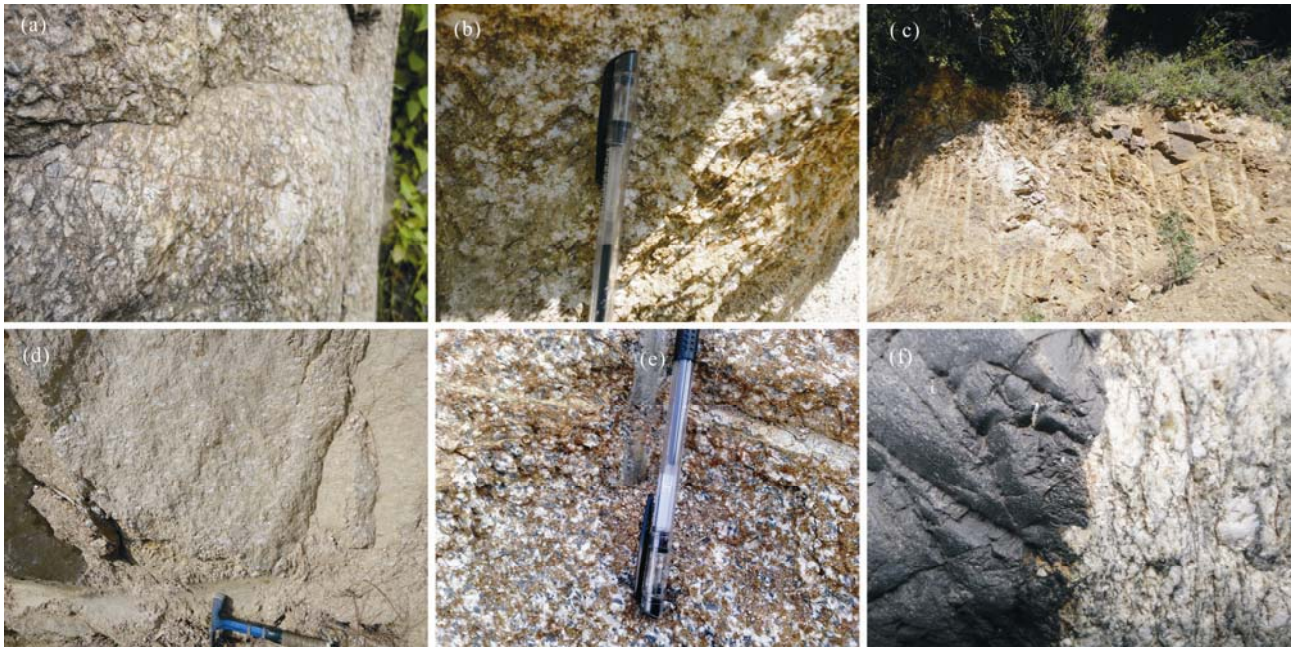


Fig. 3. The representative optical field photographs of the granitoids from this study. (a), Biotite monzogranite from S-type granite; (b), Biotite monzogranite from I-type granite; (c), Monzonitic granite from S-type granite; (d), Biotite granodiorite from S-type granite; (e), Quartz diorite from I-type granite; (f), The contact of the Biotite monzogranite (S-type) and gabbro.

Table 2. All the analyzed samples have distinguishable geochemistry features and can be divided into two groups.

For group A, their SiO_2 contents range from 42.04%–52.08%, with an average of 49.19%, whereas the A/CNK cover a restricted range between 0.57% and 0.87%, and the $\text{Na}_2\text{O}/\text{K}_2\text{O}$ ratios from 1.14 to 10.55. They exhibit variable contents of FeO (5.16%–12.55%) and Fe_2O_3 (2.1%–5.08%). They are characterized by high MgO (4.73%–7.55%, with an average of 6.02%), CaO (8.24%–9.53%, with an average of 9%), Na_2O (2.1%–3.48%, with an average of 2.79%), TiO_2 (1.07%–2.83%, with an average of 1.74%) and low K_2O (0.33%–1.98%, with an average of 1.21%). Samples from group A have high LOI (loss on ignition) values between 1.06% and 2.6%, indicating high degree of post-magmatic chemical alteration (Chen et al., 2015).

Group B are peraluminous with the limited A/CNK ratios between 1.25 and 1.71, and with the CIPW normative corundum $>1\%$. Compared to group A, group B are characterized by higher SiO_2 (69.55%–76.42%) and K_2O (1.97%–5.52%, an average of 4.52%), but with relatively lower FeO (0.65%–4.38%), Fe_2O_3 (0.51%–1.47%), MgO (0.11%–1.16%, an average of 0.69%), CaO (0.36%–1.28%, an average of 0.76%) and TiO_2 (0.05%–0.7%, an average of 0.42%).

Based on the geochemistry characters, both group A and group B granites can be well distinguished as the I-type granite and as the S-type granite, respectively, which were defined by Chappell and White (Chappell et al., 2001; Gao et al., 2016). They can also be distinguished in

some of the major element plots (Fig. 4a–d).

5.2 Trace elements

Trace element compositions of the samples are listed in Table 3. Group A show very uniform chondrite-normalized REE pattern and $(\text{La}/\text{Yb})_N = 1.84\text{--}6.49$ with slight negative Eu anomalies ($\text{Eu}/\text{Eu}^* = 0.83\text{--}0.93$), with the except of the D3052 sample without Eu anomalies ($\text{Eu}/\text{Eu}^* = 0.99$) and the D3050 sample with slight positive Eu anomalies ($\text{Eu}/\text{Eu}^* = 1.2$) (Fig. 5b). They are characterized by the enrichment of highly incompatible elements (such as K, Rb, Ba, Th) and LREEs such as Ce, relative to those of MORB (Fig. 5a). An inference could be drawn that the parent magmas of group A granites come from mantle directly and contaminated continental crust in the fractionation and assimilation processes during magma ascent and emplacement (Husen et al., 2016; Yin et al., In press).

The group B granites are enriched in LREEs relative to HREEs with $(\text{La}/\text{Yb})_N$ ratios of 3.85–18.56. The REE pattern shows all samples come from one magma source and underwent a high degree of fractionation with strongly negative Eu anomalies ($\text{Eu}/\text{Eu}^* = 0.38\text{--}0.66$) and various total REE from 56.03 to 816.56 (Fig. 5d). In the MORB-normalized trace element variation diagram, all the samples are enriched in large ion lithophile elements (LILEs, such as Rb, Th and K) and LREEs such as Ce, and depleted in high field strength elements (HFSEs, such as Nb and Ti), with negative Sr and Ti anomalies (Fig. 5c), consistent with the geochemical characteristics of

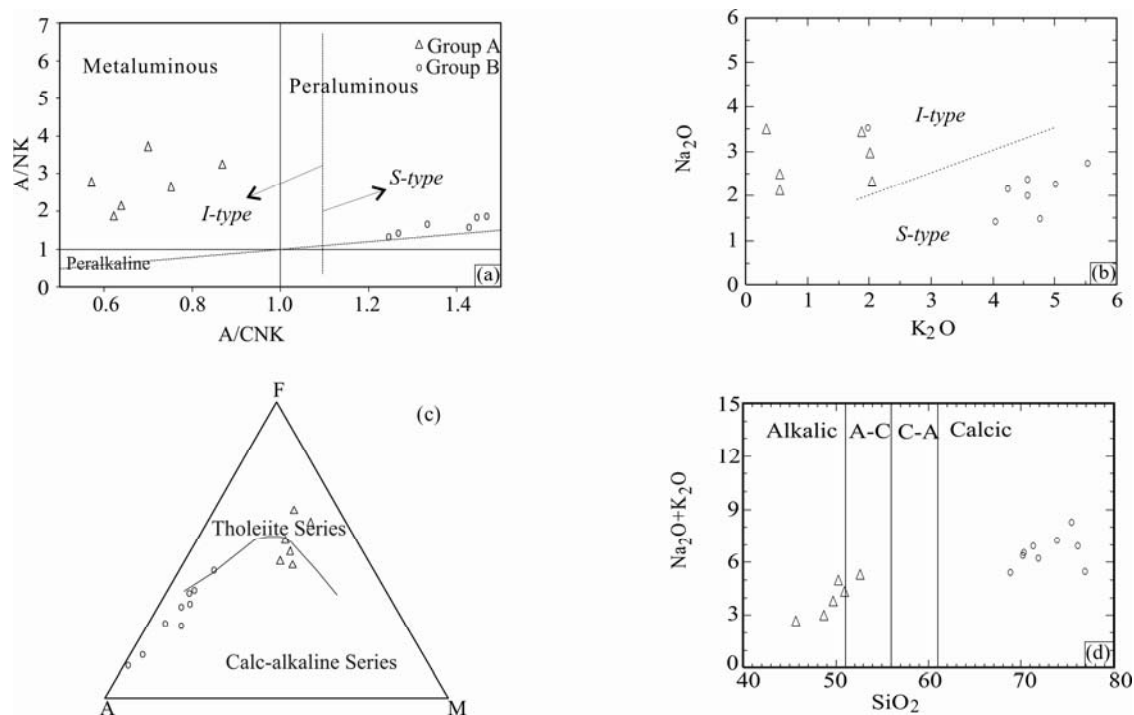


Fig. 4. Major oxides discrimination diagrams for two types of granite from Dechang county, Sichuan province within the western Yangtze Block.

(a), A/NK- A/CNK diagram is from Shand (1943) and was modified by Jamil et al. (2016); (b), Na_2O - K_2O diagram is from Chappell et al. (2001); (c), AFM diagram is from Irvine et al. (1971); (d), $(\text{Na}_2\text{O}+\text{K}_2\text{O})$ - SiO_2 diagram is from Peacock (1931).

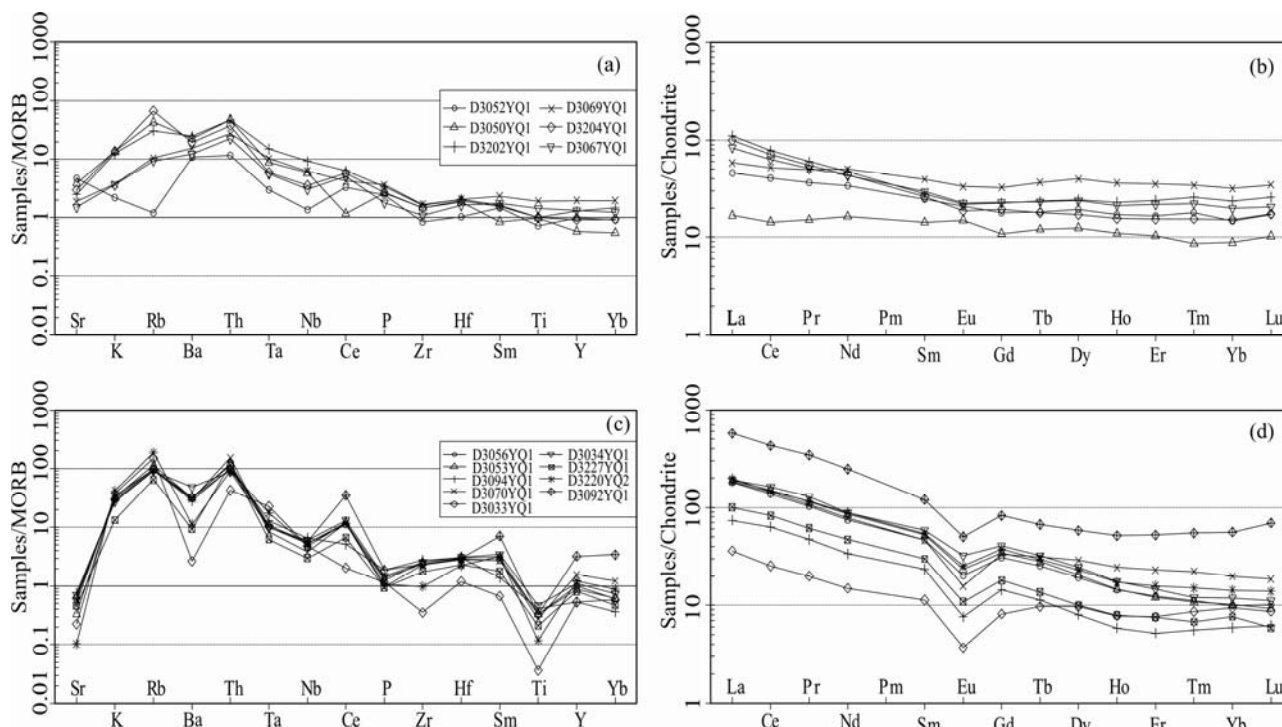


Fig. 5. MORB normalized spidergrams for the group A granites (a) and group B granites (c). Normalizing values are from Pearce (1983). Chondrite normalized REE patterns for the group A granites (b) and group B granites (d). Normalizing values are from Boynton (1984).

magma derived from the melting of continental crust.

5.3 Zircon U-Pb dating

The LA-MC-ICPMS and LA-ICP-MS U-Th-Pb

analytical data for zircons of the samples from the western Yangtze Block are shown in Table 4 and Table 5, and graphically presented on concordia U-Pb diagrams in Fig. 6 and Fig. 7. Cathodo-luminescence (CL) images of zircon

Table 3 Trace element (ppm) compositions for two types of Granite in the western Yangtze Block

	S-type granite									I-type granite					
	D3033	D3034	D3053	D3056	D3070	D3092	D3094	D3220	D3227	D3050	D3052	D3067	D3069	D3202	D3204
Pb	40.2	30.3	17.7	17	29.9	38.5	32.3	14.2	7.21	19.4	14.6	16.2	13.2	15.8	14
Zn	30.3	85.6	604	306	49.2	73.8	86.8	16.8	22.7	102	104	75.4	132	99.9	98.7
Cr	10.7	41.9	20.6	36	17.7	19.4	32.2	7.02	17.6	208	33.4	166	120	105	228
Ni	3.7	18.1	9.12	8.76	6.76	11.1	11.4	1.62	5.29	78.4	18	49.2	23.4	32.9	12.4
Co	0.96	12.3	6.5	7.14	6.08	6.99	9.44	3.95	3.18	39	29.9	51.3	47.8	38.7	35.4
Rb	299	180	224	192	194	194	184	372	128	85.8	2.42	18.7	20.8	61.4	134
Sr	26.8	83.6	40.2	79.1	62.1	74.6	92.6	12.3	55.4	460	566	178	224	298	354
Ba	53.4	962	628	644	592	626	556	222	185	450	214	242	306	493	390
V	13.6	57.3	40.5	45.1	34.6	38.6	42.5	15	28	208	188	282	365	238	186
Nb	17	21.1	18.4	18.7	13.3	20.2	22.7	16.9	10.5	20.4	4.78	10.6	21.8	32.1	12.5
Ta	4.04	1.77	1.93	1.81	1.49	1.88	2.31	3.14	1.12	1.58	0.53	1	1.83	2.7	1.06
Zr	31.8	228	230	212	207	214	248	88.6	159	132	75.8	97.8	150	144	132
Hf	2.9	7.44	7.36	6.95	6.72	7.16	7.36	5.41	5.56	4.37	2.46	3.86	4.92	4.87	4.69
U	4.7	3.42	5.44	3.98	5.15	4.64	6.44	7.2	4.57	2.27	1.08	1.35	2.59	3.54	1.94
Th	8.43	17.6	23.8	22.6	30.4	19.2	20	17.9	23	9.44	2.32	4.45	5.46	9.24	7.48
La	11.2	59.2	55	55.9	56.5	60.9	58.1	22.8	48.2	34.2	14.2	47.8	18	34.4	25.8
Ce	20.5	130	110	110	116	117	120	51.2	96.5	69.8	32.6	97.5	42.1	62.8	51
Pr	2.44	15.6	13	12.4	13.1	14	13.8	5.76	11.2	7.7	4.44	11.2	6.03	7.32	6.2
Nd	8.98	53	47.1	44.9	46.5	52.8	50.9	20.2	40.2	30.8	20.2	42.8	30.1	28.3	25.7
Sm	2.22	11.4	9.54	9.11	9.04	10.5	10.2	4.58	8.17	5.83	4.82	8.49	7.69	5.4	5.72
Eu	0.27	2.38	1.42	1.49	1.16	1.86	1.72	0.56	0.98	1.52	1.53	1.67	2.44	1.61	1.64
Gd	2.12	10.5	8.42	8	8.66	9.68	8.94	3.75	6.65	6.02	4.62	7.8	8.42	5.84	5.87
Tb	0.46	1.54	1.26	1.2	1.48	1.41	1.33	0.54	0.86	1.04	0.86	1.19	1.74	1.11	1.1
Dy	3.14	7.94	6.5	6.21	9.32	7.48	6.59	2.6	3.97	7.14	6.18	6.41	12.8	7.84	7.68
Ho	0.56	1.26	1.08	1.04	1.76	1.24	1.06	0.42	0.67	1.47	1.22	1.13	2.59	1.65	1.53
Er	1.6	3.08	2.69	2.61	4.85	3.34	2.53	1.09	1.8	4.32	3.46	2.99	7.39	5.02	4.57
Tm	0.28	0.39	0.38	0.36	0.72	0.49	0.35	0.18	0.26	0.71	0.58	0.43	1.11	0.83	0.72
Yb	1.98	2.49	2.37	2.06	4.16	3	2.13	1.24	1.89	4.46	3.08	2.76	6.61	4.93	4.14
Lu	0.28	0.36	0.34	0.33	0.6	0.45	0.3	0.2	0.28	0.78	0.55	0.41	1.11	0.83	0.66
Y	16	33.5	30.4	29.9	47.2	36.6	26.6	15.8	26.6	36.4	29.4	30.3	58.3	38.3	39.3

Table 4 U-Pb data for zircons from I-type granite in the western Yangtze Block

Grain No.	Pb	U	Isotopic ratio					Age (Ma)						
			$^{206}\text{Pb}/^{238}\text{U}$	1σ	$^{207}\text{Pb}/^{235}\text{U}$	1σ	$^{207}\text{Pb}/^{206}\text{Pb}$	1σ	$^{206}\text{Pb}/^{238}\text{U}$	1σ	$^{207}\text{Pb}/^{235}\text{U}$	1σ	$^{207}\text{Pb}/^{206}\text{Pb}$	1σ
1	67.42829	512.92516	0.13877	0.00106	1.28699	0.02024	0.06726	0.00106	837.7	6.4	840	13.2	845.9	32.9
2	99.47376	912.11972	0.08682	0.00062	0.73417	0.01100	0.06133	0.00085	536.7	3.9	559	8.4	650.7	29.8
3	195.87282	2085.95749	0.08955	0.00068	0.72817	0.01088	0.05898	0.00083	552.9	4.2	555.5	8.3	566.2	30.8
4	163.90252	1341.29807	0.11960	0.000833	1.05381	0.01577	0.06390	0.00088	728.3	5.1	730.8	10.9	738.4	29.2
5	166.2809	1115.7975	0.13919	0.00106	1.28675	0.02281	0.06705	0.001	840.1	6.4	839.9	14.9	839.2	31.0
6	261.17497	2048.8626	0.13050	0.00103	1.18227	0.01897	0.06571	0.00096	790.7	6.2	792.4	12.7	797	30.8
7	368.44167	3326.68033	0.10413	0.0007	0.88226	0.01359	0.06145	0.00087	638.6	4.3	642.2	9.9	655	30.3
8	183.28195	1289.91973	0.13855	0.00094	1.28226	0.02265	0.06712	0.00113	836.4	5.7	837.9	14.8	841.6	35
9	476.45991	4438.33933	0.10426	0.0009	0.88085	0.015	0.06128	0.00088	639.3	5.5	641.4	10.9	649	30.7
10	579.88289	5960.27005	0.09647	0.00066	0.79365	0.01291	0.05967	0.00092	593.7	4.1	593.2	9.6	591.5	33.5
11	52.35608	366.00472	0.13903	0.00093	1.28728	0.01944	0.06715	0.00094	839.2	5.6	840.1	12.7	842.5	29.1
12	109.26178	796.40409	0.13286	0.001	1.20827	0.01821	0.06596	0.00089	804.2	6.1	804.4	12.1	805	28.1
13	292.25819	2683.19113	0.11145	0.00131	0.96107	0.01816	0.06254	0.00086	681.1	8.0	683.9	12.9	692.8	29.4
14	471.74838	5436.65712	0.08585	0.00071	0.68745	0.00533	0.05808	0.00079	531	4.4	531.3	4.1	532.6	29.9
15	557.08935	4198.30262	0.13847	0.001	1.28259	0.02278	0.06718	0.00122	836.0	6.0	838.0	14.9	843.2	37.8
16	48.4249	370.31556	0.12329	0.00084	1.09743	0.01953	0.06456	0.00106	749.4	5.1	752.1	13.4	760.0	34.6
17	63.38542	454.78939	0.13906	0.00092	1.28882	0.02426	0.06722	0.00118	839.4	5.6	840.8	15.8	844.5	36.6
18	78.48415	554.33754	0.13814	0.0009	1.27635	0.01946	0.06701	0.00094	834.1	5.5	835.2	12.7	838.1	29.1
19	89.28909	761.00384	0.12404	0.00081	1.14336	0.0189	0.06685	0.00104	753.8	4.9	774.1	12.8	833.2	32.4
20	55.28251	373.57812	0.13817	0.00089	1.27268	0.01901	0.0668	0.00091	834.3	5.4	833.6	12.4	831.7	29
21	134.77349	945.0223	0.13959	0.00101	1.29368	0.01921	0.06722	0.00095	842.3	6.1	842.9	12.5	844.5	29.3
22	139.03276	1124.82994	0.12172	0.00125	1.07289	0.01808	0.06393	0.00097	740.5	7.6	740.2	12.5	739.2	32
23	430.27281	3847.44436	0.1125	0.0008	0.96521	0.01464	0.06223	0.00086	687.2	4.9	686	10.4	681.9	29.6
24	105.27293	792.7033	0.12996	0.0012	1.17745	0.02401	0.06571	0.00121	787.7	7.3	790.1	16.1	797.1	38.6
25	31.291936	268.28412	0.11236	0.00075	0.96756	0.01723	0.06245	0.00104	686.4	4.6	687.2	12.2	689.7	35.6

grains from the individual selected rock samples are shown in Fig. 6 and Fig. 7 as well.

Sample D3202: The zircon grains are euhedral to subhedral, and prismatic, varying from short to elongate. They vary in lengths from 70 μm to 240 μm (Fig. 6). The CL images indicate that some of the zircons show oscillatory zoning, whereas some do not present obvious

cores and rims (Fig. 6). Nine out of twenty-five analyzed spots of these zircons yield a weighted mean $^{206}\text{U}/^{238}\text{U}$ age of 837.6 ± 3.8 Ma ($n = 9$, MSWD = 0.23) (Fig. 6), interpreted to record the crystallization age of this granite. The rest sixteen spots suffered different extents of radiogenic Pb loss possibly during the later metamorphism. The data of these spots are concordant or

Table 5 U-Pb data for zircons from S-type granite in the western Yangtze Block

Grain No.	Th (ppm)	U (ppm)	Isotopic ratio						Age (Ma)						Conc.%
			$^{207}\text{Pb}/^{206}\text{Pb}$	1σ	$^{207}\text{Pb}/^{235}\text{U}$	1σ	$^{206}\text{Pb}/^{238}\text{U}$	1σ	$^{207}\text{Pb}/^{206}\text{Pb}$	1σ	$^{207}\text{Pb}/^{235}\text{U}$	1σ	$^{206}\text{Pb}/^{238}\text{U}$	1σ	
Zircon U-Pb isotopes for sample D3070															
D3070-01	289.05612	2303.527	0.07563	0.00208	1.74047	0.04787	0.16536	0.00159	1087	55.1	1023.6	17.7	986.5	8.8	96%
D3070-02	397.82801	3292.80765	0.07251	0.00197	1.51166	0.04007	0.14983	0.00138	1011.1	54.8	935.1	16.2	900	7.7	96%
D3070-03	350.51762	2937.7146	0.07472	0.00184	1.67285	0.04093	0.16076	0.00169	1061.1	49.2	998.3	15.6	961	9.4	96%
D3070-04	453.9715	2709.75585	0.07128	0.00195	1.59322	0.04426	0.16036	0.00193	964.8	55.6	967.6	17.3	958.8	10.7	99%
D3070-05	549.43777	2312.74205	0.07661	0.00222	1.76697	0.0496	0.16563	0.00171	1110.8	57.4	1033.4	18.2	988	9.5	95%
D3070-06	243.23036	1622.33363	0.07339	0.00239	1.70048	0.05416	0.16632	0.00194	1033.3	66.7	1008.7	20.4	991.8	10.7	98%
D3070-07	314.65303	2635.58356	0.0722	0.00222	1.66134	0.05036	0.16511	0.00177	990.7	63	993.9	19.2	985.1	9.8	99%
D3070-08	526.70652	2836.69092	0.07257	0.00206	1.60663	0.044	0.15925	0.00158	1011.1	57.9	972.8	17.1	952.6	8.8	97%
D3070-09	862.04679	3530.15882	0.07819	0.00258	1.60664	0.0541	0.14749	0.00142	1151.6	65.9	972.8	21.1	886.9	8	90%
D3070-12	805.72982	3429.0299	0.07175	0.00214	1.49699	0.04458	0.15026	0.00151	988.9	61.1	929.2	18.1	902.4	8.5	97%
D3070-13	4272.2079	62713.18956	0.07141	0.00214	1.16986	0.04291	0.1182	0.00292	968.515	61.9	786.6	20.1	720.2	16.8	91%
D3070-14	276.60349	2161.14971	0.07538	0.00216	1.665	0.0497	0.15851	0.0019	1079.6	62	995.3	18.9	948.5	10.6	95%
D3070-15	339.16726	2451.18104	0.07387	0.00207	1.74531	0.04898	0.16969	0.00196	1038.9	52.8	1025.4	18.1	1010.4	10.8	98%
D3070-16	319.43569	2441.51357	0.07696	0.00246	1.75105	0.05745	0.16259	0.00154	1120.4	64	1027.5	21.2	971.2	8.6	94%
D3070-17	359.47757	2594.99793	0.07027	0.00236	1.62843	0.05196	0.16586	0.00166	936.1	70.4	981.3	20.1	989.3	9.2	99%
D3070-18	273.08867	2286.3410	0.07098	0.00273	1.62979	0.05921	0.16401	0.00175	966.7	79.6	981.8	22.9	979	9.7	99%
D3070-19	395.19227	4074.28152	0.0709	0.00277	1.34741	0.04935	0.13561	0.00138	953.7	80.1	866.4	21.4	819.8	7.8	94%
D3070-20	444.47537	3096.98539	0.06936	0.00254	1.26905	0.04633	0.13054	0.0019	909.3	75.9	832	20.7	790.9	10.8	94%
D3070-21	662.30685	3751.12022	0.06947	0.00263	1.34329	0.04117	0.13813	0.00149	922.2	61	864.7	17.8	834.1	8.4	96%
D3070-22	248.0785	2581.58929	0.07022	0.00212	1.58181	0.04563	0.16125	0.00181	1000	61.6	963.1	17.9	963.7	10	99%
D3070-23	408.19578	3464.80829	0.07034	0.00199	1.56103	0.04397	0.15875	0.00195	938.9	57.4	954.9	17.4	949.8	10.8	99%
D3070-24	351.63234	2516.20487	0.07076	0.00194	1.65281	0.04475	0.16702	0.0018	950	55.6	990.6	17.1	995.7	10	99%
Zircon U-Pb isotopes for sample D3034															
D3034-02	85.785347	1132.23856	0.07335	0.00221	1.71358	0.05165	0.16788	0.00204	1033.3	61.1	1013.6	19.3	1000.4	11.2	98%
D3034-03	136.97296	557.39933	0.07094	0.00262	1.63404	0.0602	0.16586	0.00236	966.7	74.8	983.4	23.2	989.3	13	99%
D3034-04	241.00002	463.90534	0.07199	0.00327	1.79621	0.07853	0.18127	0.00233	987	88	1044.1	28.5	1073.9	12.7	97%
D3034-05	88.23786	649.43667	0.06972	0.00271	1.71066	0.06709	0.17665	0.00238	920.4	79.6	1012.5	25.1	1048.7	13	96%
D3034-06	140.47614	689.93945	0.067153	0.00272	1.59739	0.06528	0.17116	0.00209	842.6	78.7	969.2	25.5	1018.5	11.5	95%
D3034-07	517.48904	996.03121	0.07143	0.00268	1.60086	0.05678	0.16262	0.00201	969.4	77.8	970.5	22.2	971.3	11.1	99%
D3034-08	156.74764	679.72451	0.07069	0.00260	1.66368	0.06236	0.16984	0.00201	950	74.8	994.8	23.8	1011.2	11.1	98%
D3034-09	135.5047	608.64549	0.07143	0.00272	1.63652	0.06047	0.16663	0.0021	969.4	77.8	984.4	23.3	993.5	11.6	99%
D3034-10	178.30747	645.33728	0.07143	0.00255	1.64515	0.05598	0.16788	0.00188	970.1	74.1	987.7	21.5	1000.4	10.4	98%
D3034-11	22.89104	1044.75667	0.06867	0.00228	1.5904	0.05314	0.16761	0.0019	888.6	73.1	966.5	20.8	998.9	10.5	96%
D3034-12	146.01436	190.02594	0.07326	0.00428	1.90296	0.1055	0.19125	0.00338	1020.4	123.2	1082.1	36.9	1128.2	18.3	95%
D3034-13	143.4113	457.01248	0.07246	0.00288	1.69604	0.06691	0.17025	0.00212	998.2	80.4	1007	25.2	1013.5	11.7	99%
D3034-14	557.82503	1117.20082	0.07533	0.00238	1.7362	0.05464	0.16685	0.00177	1077.5	63	1022	20.3	994.7	9.8	97%
D3034-15	694.37583	808.62363	0.07718	0.00252	1.77259	0.05737	0.16604	0.00185	1125.6	64.8	1035.5	21	990.2	10.2	95%
D3034-16	256.73646	471.91423	0.07238	0.00317	1.69433	0.07126	0.1705	0.00226	998.2	88.9	1006.4	26.9	1014.8	12.4	99%
D3034-17	237.55267	923.18831	0.07379	0.00249	1.74112	0.05871	0.17025	0.00203	1035.2	68.2	1023.9	21.8	1013.5	11	98%
D3034-18	189.24439	1414.75103	0.07128	0.00212	1.70197	0.05253	0.17177	0.00227	964.8	59.7	1009.3	19.7	1021.9	12.5	98%

nearly concordant, which show various age groups and may indicate polymetamorphism.

Sample D3070: The zircon grains in this sample are euhedral with good terminations (Fig. 7a). They show variable grain sizes (60 μm –180 μm) with the length/wide ratios of 6:1–2:1 (Fig. 7a). They have the Th/U ratios range from 0.12 to 0.69. Twenty-two analyzes were performed on 22 selected zircons (Table 5). When plotted on the Concordia diagram (Fig. 7a), the regression involving all the 22-date points yield an upper intercept age of 1055 \pm 43 Ma and a lower intercept age of 272 \pm 240 Ma (MSWD = 1.06). The upper intercept age of 1055 \pm 43 Ma is indistinguishable from the U-Pb concordant age of 1039 \pm 53 Ma obtained from the analysis D3070-15 (Table 5). The 1055 \pm 43 Ma age is interpreted as the intrusion age of the granite.

Sample D3034: The zircon grains are euhedral to subhedral with ovoid shapes (Fig. 7b). Some of the zircons show good oscillatory zoning and have Th/U ratios

between 0.50 and 0.86, typical of zircons crystallized from an igneous melt. Nine analyzes were conducted on 9 selected zircon grains (Table 5). When plotted on a Concordia diagram (Fig. 7b), the 9 data points defined a linear array yielding an upper intercept age of 1031 \pm 77 Ma and a lower intercept age of 482 \pm 1200 Ma (MSWD=1.01). The upper intercept age of 1031 \pm 77 Ma is indistinguishable from two concordant ages of 1033 \pm 61 Ma and 1035 \pm 68 Ma obtained from analysis of D3034-02 and D3034-17, respectively (Table 5). The upper intercept age of 1031 \pm 77 Ma is therefore interpreted to record the crystallization age of this granite.

5.4 Sm-Nd systematics

Six selected samples include three biotite monzogranites (D3052, D3070, D3286), one monzonitic granite (D3053), and two quartz diorites (D3202 and D3069). The samples are divided into two groups (group A and group B), based on the study of their geochemistry

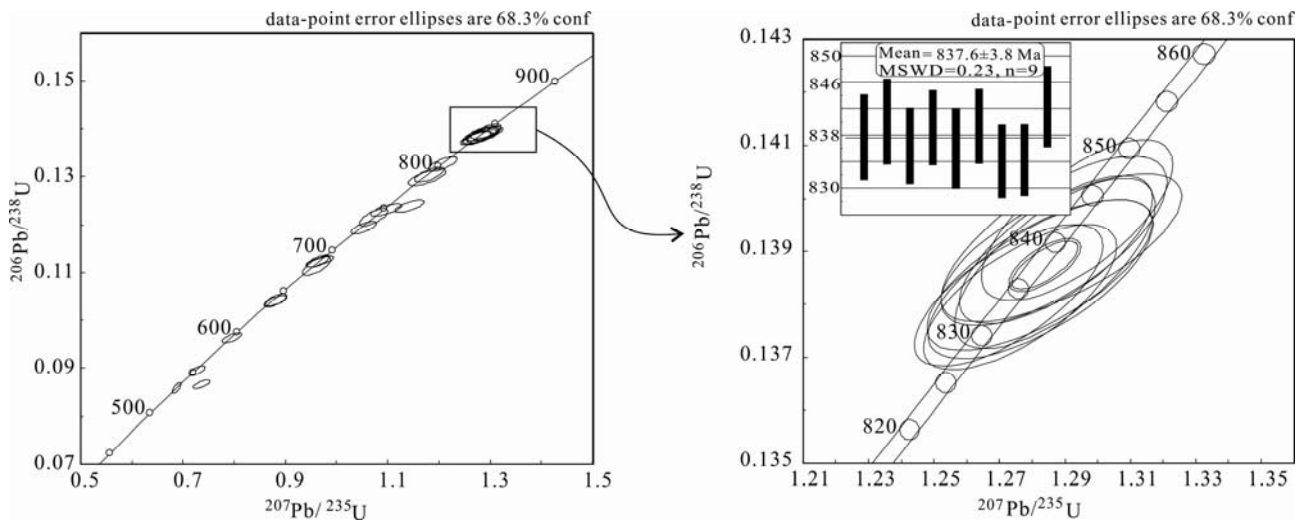


Fig. 6. U-Pb Concordia diagram for dated zircon sample D3202.

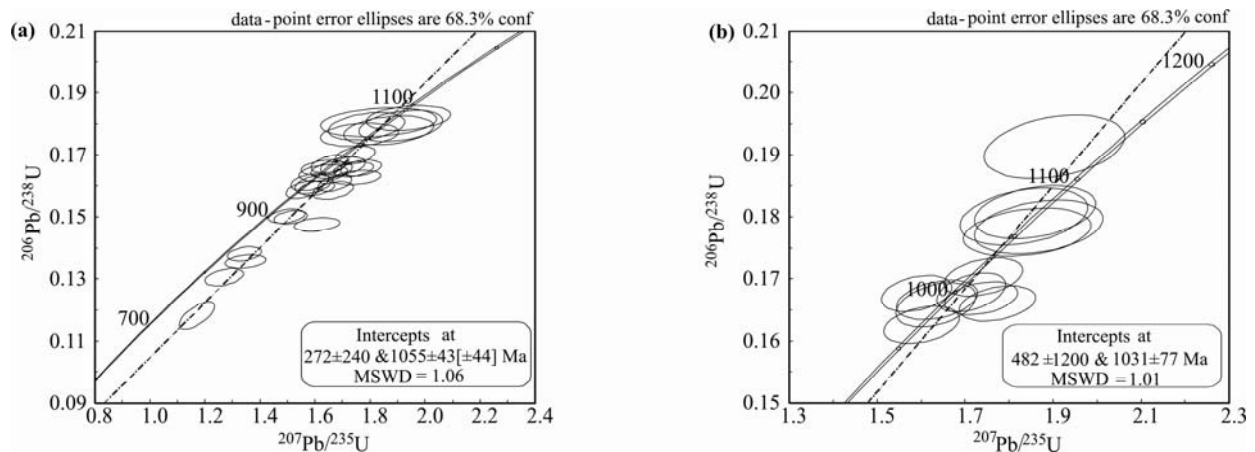


Fig. 7. U-Pb Concordia diagrams for dated zircon sample D3070 (a) and sample D3034 (b).

and geochronology. Group A and group B have representative ages of 837.6 ± 3.8 Ma for the I-type granite, and 1055 ± 43 Ma for the S-type granite, respectively.

The Nd isotope compositions of samples are presented in Table 6. The depleted mantle (t_{DM}) ages are also shown in Table 6, which are calculated using the present mantle, $^{143}\text{Nd}/^{144}\text{Nd}$ and $^{147}\text{Sm}/^{144}\text{Nd}$ ratio values of 0.51316 and 0.2137 respectively (Goldstein et al., 1984; Peucat et al., 1988). Age calculations are based on a decay constant of $6.54 \times 10^{-12}\text{yr}^{-1}$ (Steiger et al., 1977) whereas the ϵ_{Nd} values are calculated using the zircon U–Pb emplacement ages reported in this study.

The Nd isotope data of the rocks of group A have similar $^{143}\text{Nd}/^{144}\text{Nd}$ ratios between 0.51192 and 0.51195, corresponding to initial ϵ_{Nd} ($t = 837$ Ma) values of 1.22 to 5.63. Calculated t_{DM} ages yield the values from 1.0 to 1.38 Ga and the $t_{DM,2stg}$ ages yield values from 0.99 to 1.06 Ga, however, the D3069 gives a t_{DM} age of 1.86 Ga with a

$t_{DM,2stg}$ age of 1.34 Ga. These data suggest that the parental magma of the granites of group A should be derived from the previously “depleted” zone—the mantle reservoir (residual solid) (Depaolo, 1988).

The group B displays $^{143}\text{Nd}/^{144}\text{Nd}$ values of 0.51241–0.51256, and gives the ϵ_{Nd} ($t = 1055$ Ma) values from (–3.29) to (–3.81). The calculated t_{DM} ages yield the values from 1.87 to 1.91 Ga with the $t_{DM,2stg}$ ages of 1.86 to 1.9 Ga, which suggested that those granites should be derived from the melting of the basement rocks with the ages between 1.91 and 1.87 Ga.

6 Discussion

6.1 Petrogenesis

Two types of spatially associated Precambrian granites in the western Yangtze Block, with different geochemical characters, have been distinguished in this study: the late Mesoproterozoic peraluminous calc-alkaline series calcic

Table 6 Sm-Nd isotopic data for two types of granite in the western Yangtze Block

Sample	Sm (ppm)	Nd (ppm)	$^{147}\text{Sm}/^{144}\text{Nd}$	$^{143}\text{Nd}/^{144}\text{Nd}$	U-Pb age*	$\epsilon_{\text{Nd}}(t)$	t_{DM} (Ga)	$t_{\text{DM,2stg}}$ (Ga)
D3052	4.802	21.06	0.138	0.512412	837	1.88	1.389	1.066
D3053	9.743	48.18	0.1224	0.511951	1055	-3.38	1.888	1.868
D3286	8.732	43.64	0.1211	0.51192	1055	-3.81	1.911	1.901
D3202	5.266	25.3	0.126	0.512538	837	5.63	1.005	0.994
D3070	8.588	43.1	0.1205	0.511942	1055	-3.29	1.865	1.861
D3069	8.605	30.42	0.1711	0.51256	837	1.22	1.875	1.34

S-type granite and the mid-Neoproterozoic metaluminous calc-alkaline series alkalic I-type granite.

Several mechanisms have been proposed to explain the genesis of I-type granite (Li et al., 2016). Chappell et al. (2001) noted that I-type granite have a broad spectrum of compositions from felsic to mafic, while the S-type granite are restricted to higher SiO_2 contents. Consistent with this observation, they pointed out that I-type granite magmas, produced by the partial melting of less-siliceous source rocks, reflect that feature in their more mafic compositions. However, Depaolo (1988) argued that I-type granite could be explained as being the end products of magmas derived from the mantle that assimilated substantial amounts of the sedimentary crustal rocks during ascent. Barbarin (1999) proposed that peraluminous granitoids are of crustal origin, calc-alkaline series granitoids are of mixed origin, and alkaline to peralkaline granitoids are of mantle origin.

These I-type granites in the western Yangtze Block, are characters of calc-alkaline series and metaluminous, and are poor in SiO_2 and K_2O but rich in Na_2O , CaO , MgO , FeO and Fe_2O_3 contents, as well as High Cr (105 ppm–228 ppm, except D3052), Ni (18 ppm–78.4 ppm) contents and $\text{CaO}/\text{Al}_2\text{O}_3$ ratios (0.5–0.7) with low SiO_2 . These characters suggest that they could have originated from the crystallization and accumulation of mantle-derived mafic magma (Renjith et al., 2016). Their REE distributions show smooth to weak right-inclined patterns with the values of $(\text{La}/\text{Yb})_{\text{N}} = 1.84\text{--}6.49$ and with the weakly negative to slightly positive Eu anomalies. They are

characterized by the enrichment of K, Rb, Ba, Th, and Ce, relative to those of MORB, consistent with the geochemical characters of EMORB. The values of $\epsilon_{\text{Nd}}(t) = 1.22\text{--}5.63$ indicate the derivation of the parental magma from depleted mantle.

The most compelling evidence to distinguishing between the effects of crustal contamination and source enrichment would be a correlation between isotopic ratios of Sr and Nd chemical compositions with a fractionation indicator (such as SiO_2 , MgO) (Wang et al., 2005; Xu et al., 2012; Gao et al., 2014). Figure 8a shows that with the increasing of SiO_2 , $\epsilon_{\text{Nd}}(t)$ values are increasing in the I-type granites, suggesting that crustal contamination has played a significant role in the petrogenesis of I-type granites. On the Th/Nb versus La/Nb diagrams (Fig. 8b), the samples from the I-type granite were plotted in the field between continental crust and MORB, suggesting that they are mixtures of mantle and subducted sources (Plank, 2005).

According to these characters, we interpret these I-type granites were resulted from the mantle-derived magma mixed with the crust material and, if any, maybe formed by assimilation and fractional crystallization as mantle-derived magma passed through preexisting crust that contained Precambrian basement (1–1.3 Ga).

The geochemical characters and mineralogical assemblages classify these S-type granites in the western Yangtze Block as CPG, in the classification of Barbarin (1999), which are granitoids of crustal origin. Our study discovers that they are peraluminous and calcic. The $\text{CaO}/$

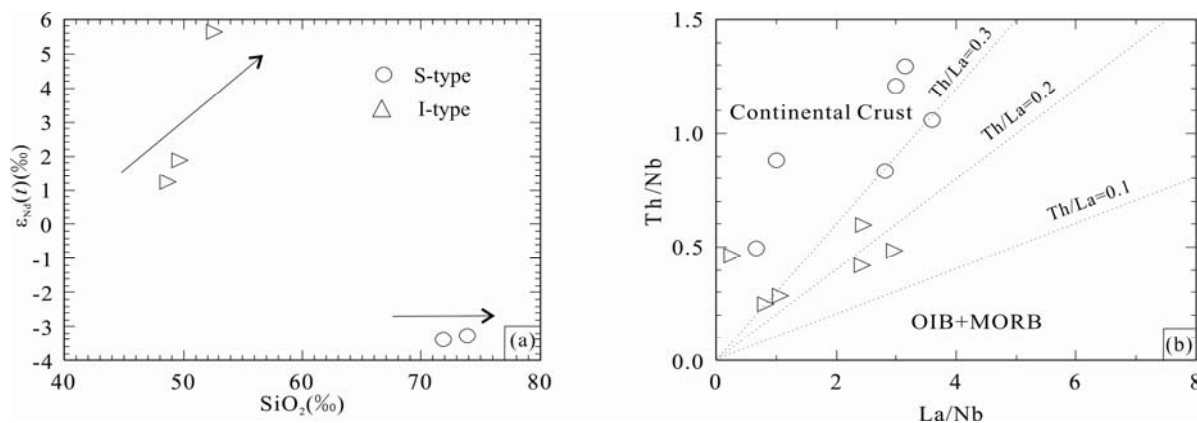


Fig. 8. Diagrams of $\epsilon_{\text{Nd}}(t)$ versus SiO_2 (a) (modified after Wang et al., 2005; Xu et al., 2012) and Th/Nb versus La/Nb (b) (after Plank, 2005).

Na_2O ratios = 0.13–0.91, indicating that the source rocks are mudstone and other clastics. The Rb/Sr ratios = 1.98–11.16 (average = 4.05), which are higher than the Rb/Sr ratios of upper crust (average = 0.32), suggesting the source rocks could come from the upper crust. The LREEs are enriched relative to HREEs, with a strongly Eu negative anomaly. There is enrichment in the large ion lithophile elements and depletion in the high field strength elements, with negative Sr and Ti anomalies. All of these geochemical characters are similar to those granites resulted from the re-melting of continental crust. The Nd isotope features indicate they should be derived from the melting of the basement rocks with the ages between 1.91 and 1.87 Ga. On the Th/Nb versus La/Nb diagrams (Fig. 8b), most of the S-type granites were plotted in the field of continental crust, suggesting the sources derived directly from the crust (Plank, 2005).

On the Sr versus Ba and Rb diagrams (Fig. 9), the S-type granites show obvious decreases in Sr, and in Ba, indicating the fractionation of K-feldspar and plagioclase, which consistent with the strong Eu depletion that requires extensive fractionation of plagioclase and/or K-feldspar. (Li et al., 2016).

6.2 Tectonic implications

The South China Craton was considered to be part of the supercontinent Rodinia although its configuration and/or precise position in the supercontinent have still been disputed (Pisarevsky et al., 2003; Li et al., 2007b; Li et al., 2008; Munteanu and Wilson, 2009; Piper, 2009; Cawood et al., 2016; Chen et al., 2016).

Two events of supercontinent assembly and dispersal have been proposed during the end of Mesoproterozoic to mid-Neoproterozoic. There is general agreement that the end of Mesoproterozoic magmatism, in the western Yangtze Block, have been produced by the collisional event of Grenville Orogeny, which caused the formation

of Rodinia (Li et al., 2008; Yao et al., 2013, 2015; Chen et al., 2014; Zhang et al., 2015; Cawood et al., 2016). However, different models have been used to interpret the tectonic setting and geodynamics of the western Yangtze Block at mid-Neoproterozoic times (Zhou et al., 2002; Zhou et al., 2006; Li et al., 2006, 2007a; Zhou et al., 2007; Munteanu and Yao, 2007; Zhao, 2008; Zhao et al., 2008; Li et al., 2008; Munteanu and Wilson, 2009; Pei Xianzhi et al., 2009; Sun, 2009; Huang et al., 2009; Dong et al., 2011; Dong et al., 2012; Du et al., 2014; Chen et al., 2015; Cui et al., 2015; Lai et al., 2015; Wu et al., 2016).

These Mesoproterozoic granites in the western Yangtze Block have been identified to be S-type according to their geochemical features of major elements as described above. In the traditional hypothesis, the S-type peraluminous granite were formed by partial melting of sedimentary rocks and/or derived from the crustal melting during collision thicken processes (Chappell et al., 2001; Mabi Awei et al., 2015; Gao et al., 2016; and references therein). In addition, according to their geochemical characters and mineralogical assemblages, these S-type granites in the western Yangtze Block affiliates to CPG, in the classification of Barbarin (1999), which are emplaced where there is thickening resulting from the convergence of two continental plates (Barbarin, 1999). In the Rb-(Yb+Ta) discrimination diagram (Fig. 10a), they plot in the syn-collision granite (syn-COLG) field, as well as nearly plotting in the syn-collision and post-orogenic fields in the R_1 - R_2 tectonic discrimination diagram (Fig. 10b). We consider it represents the span through a plate collision event, and the overlap around this area is inevitable since all granitoids evolve towards minimum melting compositions (Batchelor et al., 1985).

For these mid-Neoproterozoic I-type granites, they show metaluminous calc-alkaline characteristics, with the enrichment of highly incompatible elements (such as K, Rb, Ba, Th) and LREEs such as Ce. These features are

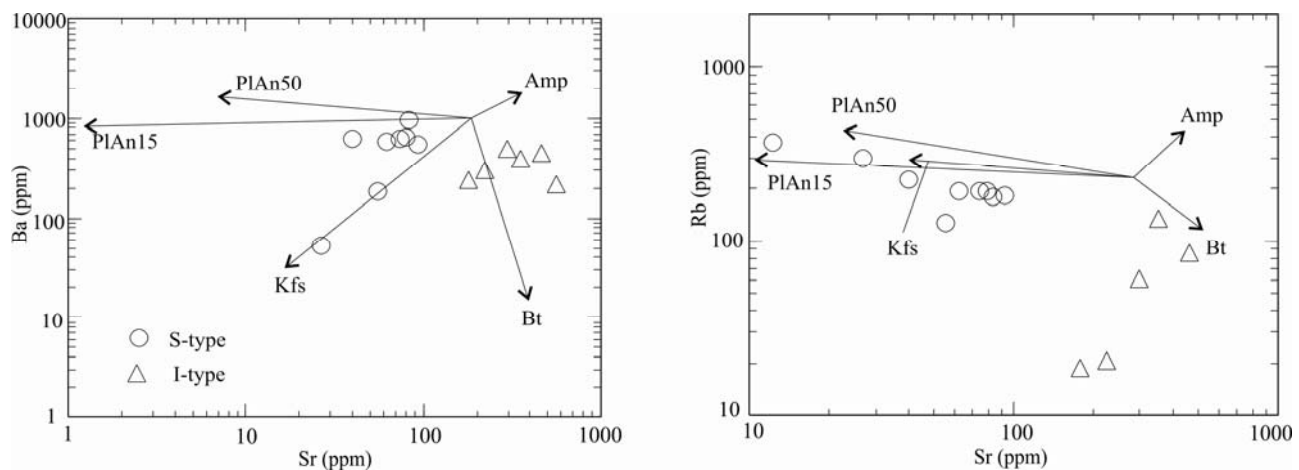


Fig. 9. Diagrams of Ba and Rb versus Sr (modified after Li et al., 2016).

consistent with the granites produced by the subduction process at the arc (Pearce et al., 1984; Pearce, 1996; Zhou et al., 2002; Zhou et al., 2006; Yin et al.; Zhao, 2008; Munteanu and Wilson, 2009). Furthermore, these I-type granites affiliate to amphibole-rich calc-alkaline granitoids (ACG) in the classification of Barbarin (1999), which are invariably emplaced above subduction zones (Barbarin, 1999). On the Rb-(Yb+Ta) discrimination diagram (Fig. 10a), they plot largely in the field of volcanic arc. In the R_1 - R_2 tectonic discrimination diagram (Fig. 10b), they nearly plot in the pre-collision field. Therefore, we interpret they were originated from the volcanic arc magmas.

6.3 Evolution and regional implications of the 1.1–0.83 Ga magmatism

Some scholars believed that the Cathaysia Block was part of Laurentia, and suggested that the collision between Laurentia-Cathaysia and Yangtze started after ca. 1149 Ma or at the end of Sibao Orogeny (Li et al., 2002; Pisarevsky et al., 2003; Li et al., 2008). It has been generally accepted that the South China Craton was formed through the amalgamation of the Yangtze and Cathaysia blocks along Sibao Orogeny (Li et al., 2002; Greentree et al., 2006; Li et al., 2010; and references therein). However, the timing of the final assembly of two blocks is still controversial (Li et al., 2002; Greentree et al., 2006; Li et al., 2007b; Li et al., 2010; Zhang et al., 2015; and references therein).

The Neoproterozoic magmatism has been thought to have been produced by a mantle plume associated with break-up of the Rodinia supercontinent (Pisarevsky et al., 2003; Li et al., 2006, 2007a; Li et al., 2008; Cui et al., 2015). However, one school of group argued that the apparent arc-signature of these Neoproterozoic igneous rocks indicate their formation in an active continental margin along the northern and western margin of Yangtze

Block which be defined as Hannan-Panxi Arc (Zhou et al., 2002; Zhou et al., 2006; Zhao, 2008; Sun, 2009; Zhao, 2010; Chen, 2013).

In this study, we obtain the 1055 ± 43 Ma age of peraluminous S-type granite which derived from the crustal re-melting and were formed in the continental collision environment. It is consistent with the worldwide Grenvillian orogenic event which were commonly associated with continental collision in the ca. 1300–900 Ma (Chen et al., 2014; and references therein). Therefore, we interpret that these late Mesoproterozoic S-type granites, in the western Yangtze Block, resulted from collision between the Yangtze and Cathaysia-Laurentia blocks –1000 Ma.

We also obtain the 837.6 ± 3.8 Ma from the metaluminous calc-alkaline series I-type granites which we identified as arc intrusions in the previous sections. However, the precise position of South China Craton, if any, in the supercontinent Rodinia at the Neoproterozoic period is hotly debated. Li et al. (1995); Pisarevsky et al. (2003); Li et al. (2008) proposed the “missing-link” model in which the South China Craton was considered as the “missing-link” between Australia-East Antarctica and Laurentia in Rodinia. On the other hand, Zhou et al. (2006) urged that Yangtze Block should have been located on the NW margin of Neoproterozoic supercontinent, rather than within it. Recently, Chen et al. (2016) suggested that the position of the pre -750Ma Yangtze Block is suspicious between the Laurentia and Australia, based on studying of U–Pb ages and Hf isotope of zircons from the late Neoproterozoic sedimentary rocks. To conclude, we interpret these metaluminous I-type granites were formed in an active continental margin arc resulted from the subduction of the oceanic lithosphere easternward (present-day orientation) underneath the western Yangtze Block at the Neoproterozoic (Fig. 11).

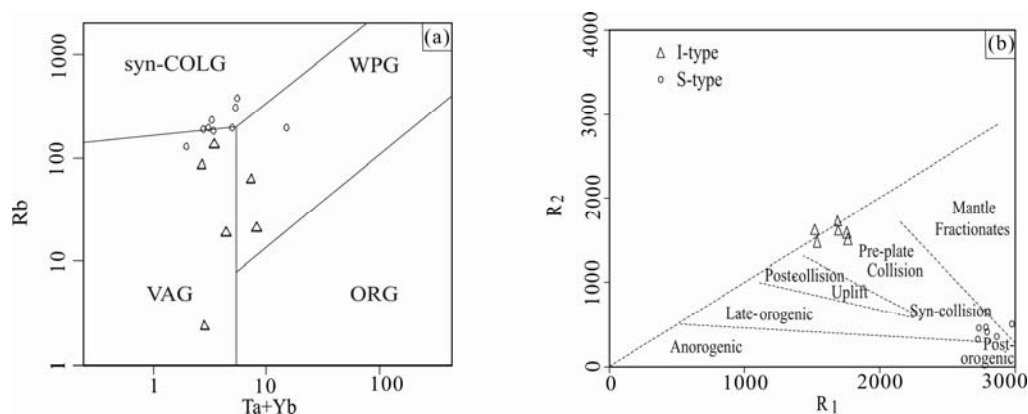


Fig. 10. Tectonic discrimination diagrams for two types of granite from Dechang county, Sichuan province within the western Yangtze Block.

(a), Rb-(Ta+Nb) diagram from Pearce et al. (1984); (b), R_1 - R_2 diagram from Batchelor et al. (1985).

7 Conclusion

(1) The geochronological data presented in this study for two types of spatially associated granites from the western Yangtze Block imply two magmatic events that occurred at 1055 ± 43 Ma and 837.6 ± 3.8 Ma, respectively. Our ages are in agreement with the other workers in the region.

(2) These Grenville-age granites are peraluminous calc-alkaline series calcic S-type granite, which resulted from the convergence of two continental plates and derived from the re-melting of the upper crustal mudstone and/or clastics. Whereas, the mid-Neoproterozoic granites are metaluminous calc-alkaline series alkalic I-type granite, which were formed in the continental arc and resulted from mantle-derived magma mixed crust material, as mantle-derived magma passed through preexisting crust that contained Precambrian basement.

(3) The collision between the Yangtze and Cathaysia blocks occurred at about 1055 Ma, consistent with the worldwide Grenvillian orogenic event. In the mid-Neoproterozoic, the oceanic lithosphere linked between Australia (?) and South China Craton eastern-ward (present-day orientation) subducted underneath the western Yangtze Block and formed N-S trend ((present-day orientation) Hannan-Panxi Arc.

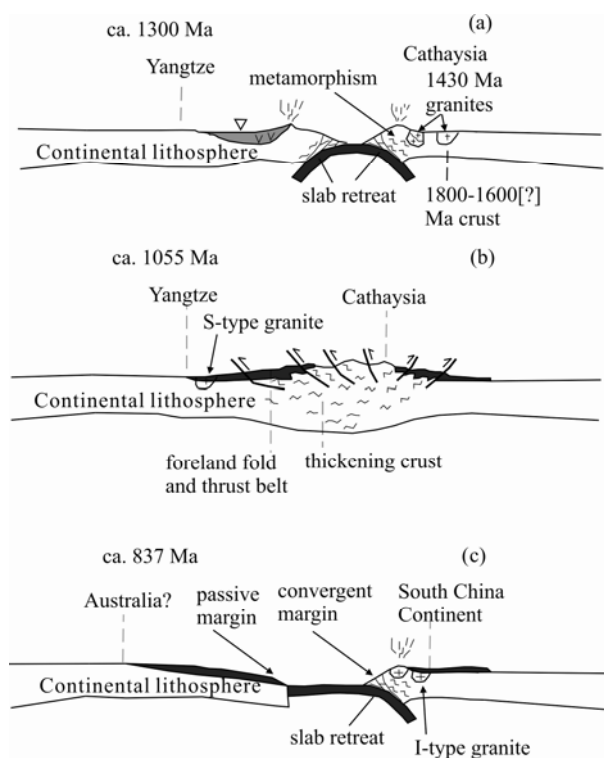


Fig. 11. A simplified model of regional tectonic evolution during 1300 Ma to 837 Ma (modified after Li et al., 2002).

Acknowledgments

We thank two anonymous reviewers for the thorough revision of the manuscript and for their insightful comments. We gratefully acknowledge Prof. Mark Allen from Durham University for his help with the English language. This study was supported by the China Geological Survey project (1212011120623). We also thank some of local geologists, Xijie Ren, Qiliang Xiao, Zhenming Chen, Yakun Yao, Daoming Cheng, Xihai Duan, Jian Zeng, Hao Chen, Wanxiong Hou, Gang Zhen, Huicheng Wu, Jihui Nong, Zihai Mise, from Panxi Team, Sichuan Bureau of Geology and Mineral Resources for their contribution to field work.

Manuscript received Sept. 13, 2016

accepted Apr. 5, 2017

edited by Fei Hongcai

References

- Barbarin, B., 1999. A review of the relationships between granitoid types, their origins and their geodynamic environments. *Lithos*, 46: 605–626.
- Batchelor, R.A., and Bowden, P., 1985. Petrogenetic interpretation of granitoid rock series using multicationic parameters. *Chemical Geology*, 48: 43–55.
- Boynton, W.V., 1984. Cosmochemistry of the rare earth elements: Meteorite studies. *Developments in Geochemistry*, 2: 63–114.
- Cawood, P.A., Strachan, R.A., Pisarevsky, S.A., Gladkochub, D.P., and Murphy, J.B., 2016. Linking collisional and accretionary orogens during Rodinia assembly and breakup: Implications for models of supercontinent cycles. *Earth and Planetary Science Letters*, 449: 118–126.
- Chappell, B.W., and White, A.J.R., 2001. Two contrasting granite types: 25 years later. *Australian Journal of Earth Sciences*, 48: 489–499.
- Chen Qiong, Sun Min, Long Xiaoping and Yuan Chao, 2015. Petrogenesis of Neoproterozoic adakitic tonalites and high-K granites in the eastern Songpan-Ganze Fold Belt and implications for the tectonic evolution of the western Yangtze Block. *Precambrian Research*, 270: 181–203.
- Chen Qiong, Sun Min, Long Xiaopin, Zhao Guochun and Yuan Chao, 2016. U–Pb ages and Hf isotopic record of zircons from the late Neoproterozoic and Silurian-Devonian sedimentary rocks of the western Yangtze Block: Implications for its tectonic evolution and continental affinity. *Gondwana Research*, 31: 184–199.
- Chen Wei, 2013. *Origin and tectonic environment of the Lala Fe-Cu(Mo, REE) deposit, Sichuan province, SW China*. Hongkong: The University of Hong Kong (Ph. D thesis): 1–273.
- Chen Wei, Sun Weihua, Wang Wei, Zhao Junhong and Zhou Meifu, 2014. “Grenvillian” intra-plate mafic magmatism in the southwestern Yangtze Block, SW China. *Precambrian Research*, 242: 138–153.
- Cui Xiaozhuang, Jiang Xinsheng, Wang Jian, Wang Xuance, Zhuo Jiwen, Deng Qi, Liao Shiyong, Wu Hao, Jiang Zhuofei

- and Wei Yanan, 2015. Mid-Neoproterozoic diabase dykes from Xide in the western Yangtze Block, South China: New evidence for continental rifting related to the breakup of Rodinia Supercontinent. *Precambrian Research*, 268, 339–356.
- Depaolo, D.J., 1988. *Neodymium isotope geochemistry: An introduction*. Springer-Verlag, 1–191.
- Dong, Yunpeng., Liu, Xiaoming., Santosh, M., Chen, Qing., Zhang, Xiaoning., Li, Wei., He, Dengfeng. and Zhang, Guowei., 2012. Neoproterozoic accretionary tectonics along the northwestern margin of the Yangtze Block, China: Constraints from zircon U–Pb geochronology and geochemistry. *Precambrian Research*, 196–197: 247–274.
- Dong Yunpeng, Liu Xiaoming, Santosh, M., Zhang Xiaoning, Chen Qing, Chen Yang and Zhao Yang, 2011. Neoproterozoic subduction tectonics of the northwestern Yangtze Block in South China: Constrains from zircon U–Pb geochronology and geochemistry of mafic intrusions in the Hannan Massif. *Precambrian Research*, 189: 66–90.
- Du Lilin, Guo Jinghui, Nutman, A.P., Wyman, D., Geng Yuansheng, Yang Chonghui, Liu Fulai, Ren Liudong and Zhou Xiwen, 2014. Implications for Rodinia reconstructions for the initiation of Neoproterozoic subduction at – 860 Ma on the western margin of the Yangtze Block: Evidence from the Guandaoshan Pluton. *Lithos*, 196–197: 67–82.
- Gao Peng, Zheng Yongfei and Zhao Zifu, 2016. Distinction between S-type and peraluminous I-type granites: Zircon versus whole-rock geochemistry. *Lithos*, 258–259: 77–91.
- Gao Xinyu, Zhao Taiping, Bao Zhiwei and Yang Alexandra Yang, 2014. Petrogenesis of the early cretaceous intermediate and felsic intrusions at the southern margin of the North China Craton: Implications for crust-mantle interaction. *Lithos*, 206–207: 65–78.
- Geng Yuansheng, Yang Chonghui, Wang Xinshe, Du Li, Ren Lillin and Zhou Xiwen, 2008. *Metamorphic basement evolution in western margin of Yangtze Block*. Beijing: Geological Publishing House, 1–215 (in Chinese with English abstract).
- Goldstein, S.L., Onions, R.K., and Hamilton, P.J., 1984. A Sm–Nd isotopic study of atmospheric dusts and particulates from major river systems. *Earth and Planetary Science Letters*, 70: 221–236.
- Greentree, M.R., Li Zhengxiang, Li Xianhua and Wu Huaichun, 2006. Late Mesoproterozoic to earliest Neoproterozoic basin record of the Sibao orogenesis in western South China and relationship to the assembly of Rodinia. *Precambrian Research*, 151: 79–100.
- Greentree, M.R., and Li Zhengxiang, 2008. The oldest known rocks in south-western China: SHRIMP U. *Journal of Asian Earth Sciences*, 33: 289–302.
- Huang Xiaolong, Xu Yigang, Lan Jianbo, Yang Qijun and Luo Zhengyu, 2009. Neoproterozoic adakitic rocks from Mopanshan in the western Yangtze Craton: Partial melts of a thickened lower crust. *Lithos*, 112: 367–381.
- Husen, A., Kamenetsky, V.S., Everard, J.L., and Kamenetsky, M.B., 2016. Transition from ultra-enriched to ultra-depleted primary MORB melts in a single volcanic suite (Macquarie Island, SW Pacific): Implications for mantle source, melting process and plumbing system. *Geochimica et Cosmochimica Acta*, 185: 112–128.
- Irvine, T.N., and Baragar, W.R.A., 1971. A guide to the chemical classification of the common volcanic rocks. *Canadian Journal of Earth Sciences*, 8: 523–548.
- Jamil, A., Ghani, A.A., Zaw, K., Osman, S., and Quek, L.X., 2016. Origin and tectonic implications of the ~200 Ma, collision-related Jerai pluton of the Western Granite Belt, Peninsular Malaysia. *Journal of Asian Earth Sciences*, 127: 32–46.
- Lai Shacong, Qin Jiangfeng, Zhu Renzhi and Zhao Shaowei, 2015. Neoproterozoic quartz monzodiorite-granodiorite association from the Luding-Kangding area: Implications for the interpretation of an active continental margin along the Yangtze Block (South China Block). *Precambrian Research*, 267: 196–208.
- Li Bo, Zhou Jiayi, Li Yingshu, Chen Aibing and Wang Ruixue, 2016. Geology and isotope geochemistry of the Yinchanggou-Qiluogou Pb–Zn reposit, Sichuan Province, Southwest China. *Acta Geologica Sinica (English Edition)*, 90(5): 1768–1779.
- Li Guangming, Cao Mingjian, Qin Kezhang, Evans, N.J., Hollings, P., and Seitmuratova, E.Y., 2016. Geochronology, petrogenesis and tectonic settings of pre- and syn-ore granites from the W–Mo deposits (East Kounrad, Zhanet and Akshatau), Central Kazakhstan. *Lithos*, 252–253: 16–31.
- Li Longming, 2010. *The crustal evolutionary history of the Cathaysia Block from the Paleoproterozoic to Mesozoic*. Hongkong: The University of Hong Kong (Ph. D thesis): 1–183.
- Li Xianhua, Li Zhengxiang, Sinclair, J.A., Li Wuxian and Carter, G., 2006. Revisiting the “Yanbian Terrane”: Implications for Neoproterozoic tectonic evolution of the western Yangtze Block, South China. *Precambrian Research*, 151: 14–30.
- Li Xianhua, Li Zhengxiang, Sinclair, J.A., Li Wuxian and Carter, G., 2007a. Reply to the comment by Zhou et al. on: “Revisiting the “Yanbian Terrane”: Implications for Neoproterozoic tectonic evolution of the western Yangtze Block, South China” [Precambrian Res. 151 (2006) 14–30]. *Precambrian Research*, 155: 318–323.
- Li Zhengxiang, Zhang Linghua and Powell, C.M., 1995. South China in Rodinia: Part of the missing link between Australia East Antarctica and Laurentia? *Geology*, 23: 407.
- Li Zhengxiang, Li Xianhua, Zhou Hanwen and Kinny, P.D., 2002. Grenvillian continental collision in south China: New SHRIMP U–Pb zircon results and implications for the configuration of Rodinia. *Geology*, 30: 163–166.
- Li Zhengxiang, Wartho, J.A., Occhipinti, S., Zhang Chuanli, Li Xianhua, Wang Jian and Bao Chaomin, 2007b. Early history of the eastern Sibao Orogen (South China) during the assembly of Rodinia: New mica ⁴⁰Ar/³⁹Ar dating and SHRIMP U–Pb detrital zircon provenance constraints. *Precambrian Research*, 159: 79–94.
- Li Zhengxiang, Bogdanova, S.V., Collins, A.S., Davidson, A., De Waele, B., Ernst, R.E., Fitzsimons, I.C.W., Fuck, R.A., Gladkochub, D.P., Jacobs, J., Karlstrom, K.E., Lu, S., Natapov, L.M., Pease, V., Pisarevsky, S.A., Thrane, K., and Vernikovskiy, V., 2008. Assembly, configuration, and break-up history of Rodinia: A synthesis. *Precambrian Research*, 160: 179–210.
- Li Zuochen, Pei Xianzhi, Li Ruibao, Pei Lei, Liu Chengjun, Chen Youxin, Xu Tong, Yang Jie and Wei Bo, 2015. U–Pb zircon geochronology and geochemistry of the Neoproterozoic Liujiaping Group volcanics in the northwest margin of the

- Yangtze Block: Implications for the breakup of the Rodinia supercontinent. *Acta Geologica Sinica* (English Edition), 89 (4): 1213–1225.
- Mabi Awei, Zari Muhetaer, Wen Dengkui and Zhang Mingchun, 2015. Geochemical characteristics of southern Genie ggranite in the eastern Tibet and its geological significance. *Acta Geologica Sinica*, 89: 305–318 (in Chinese with English abstract).
- Munteanu, M., and Yao Yong, 2007. The Gaojiacun intrusion: Rift- or subduction-related?: Comment on “Revisiting the “Yanbian Terrane”: Implications for Neoproterozoic tectonic evolution of the western Yangtze Block, South China” by Li et al. (2006) [Precambrian Res. 151 (2006) 14–30]. *Precambrian Research*, 155: 324–327.
- Munteanu, M., and Wilson, A., 2009. The South China piece in the Rodinian puzzle: Comment on “Assembly, configuration, and break-up history of Rodinia: A synthesis” by Li et al. (2008) [Precambrian Res. 160: 179–210]. *Precambrian Research*, 171: 74–76.
- Peacock, M.A., 1931. Classification of igneous rock series. *Journal of Geology*, 39: 54–67.
- Pearce, J.A., 1983. Role of the sub-continental lithosphere in magma genesis at active continental margins. *Journal of the Electrochemical Society*, 147: 2162–2173.
- Pearce, J.A., Harris, N., and Tindle, A.G., 1984. Trace element discrimination diagrams for the tectonic interpretation of granitic rocks. *Journal of Petrology*, 25: 956–983.
- Pearce, J., 1996. Sources and settings of granitic rocks. *Episodes*, 19: 120–125.
- Pei Xianzhi, Li Zuochen, Ding Saping, Li Ruibao, Feng Jianyun, Sun Yu, Zhang Yafeng and Liu Zhanqing, 2009. Neoproterozoic Jiaoziding peraluminous granite in the northwestern margin of Yangtze Block: Zircon SHRIMP U-Pb age and geochemistry and their tectonic significance. *Earth Science Frontiers*, 16: 231–249.
- Peucat, J.J., Jegouzo, P., Vidal, P.P., and Bernardgriffiths, J., 1988. Continental crust formation seen through the Sr and Nd isotope systematics of S-type granites in the Hercynian belt of western France. *Earth and Planetary Science Letters*, 88: 60–68.
- Piper, J.D.A., 2009. Comment on “Assembly, configuration, and break-up history of Rodinia: A synthesis” by Li et al. [Precambrian Res., 160 (2008) 179–210]. *Precambrian Research*, 174: 200–207.
- Pisarevsky, S.A., Wingate, M.T.D., Powell, C.M., Johnson, S., and Evans, D., 2003. *Models of Rodinia assembly and fragmentation*. *Geological Society*, London: Special Publications, 206: 35–55.
- Plank, T., 2005. Constraints from Thorium/Lanthanum on sediment recycling at subduction zones and the evolution of the continents. *Journal of Petrology*, 46: 921–944.
- Qi Xuexiang, Santosh, M., Zhu Luhua, Zhao Yuhao, Hu Zhaocuo, Zhang Chao and Ji Fengbao, 2014. Mid-Neoproterozoic arc magmatism in the northeastern margin of the Indochina Block, SW China: Geochronological and petrogenetic constraints and implications for Gondwana assembly. *Precambrian Research*, 245: 207–224.
- Renjith, M.L., Santosh, M., Satyanarayanan, M., Rao, D.V.S., and Tang, Li., 2016. Multiple rifting and alkaline magmatism in southern India during Paleoproterozoic and Neoproterozoic. *Tectonophysics*, 680: 233–253.
- Shand, S.J., 1927. *Eruptive rocks: Their genesis, composition, classification, and their relations to ore-deposits with a chapter on meteorites*. London: Thomas Murby and Company, 1–479.
- Steiger, R.H., and Jager, E., 1977. Subcommission on geochronology: Convention on the use of decay constants in geochronology and cosmochronology. *Earth and Planetary Science Letters*, 36: 359–362.
- Sun Weihua, 2009. *The Neoproterozoic Yanbian group and associated plutons in the western Yangtze Block, SW China*. Hongkong: The University of Hong Kong (Ph. D thesis): 1–224.
- Sun Ya, Liu Jianxin, Tang Youcai, Chen Jiawei, Zhou Keping and Chen Bo, 2016. Structure of the upper Mantle and transition zone beneath the South China Block imaged by finite frequency tomography. *Acta Geologica Sinica* (English Edition), 90(5): 1637–1652.
- Wang Xinshui, Gao Jun, Klemd, R., Jiang Tuo, Zhai Qingguo, Xiao Xuchang and Liang Xinquan, 2015. Early Neoproterozoic multiple arc-back-arc system formation during subduction-accretion processes between the Yangtze and Cathaysia blocks: New constraints from the supra-subduction zone NE Jiangxi ophiolite (South China). *Lithos*, 236–237: 90–105.
- Wang Xiaolei, Zhou Jiancheng, Qiu Jiansheng and Gao Jianfeng, 2004. Geochemistry of the Meso- to Neoproterozoic basic-acid rocks from Hunan Province, South China: Implications for the evolution of the western Jiangnan Orogen. *Precambrian Research*, 135: 79–103.
- Wang Yuejun, Fan Weiming, Peng Touping, Zhang Hongfu and Guo Feng, 2005. Nature of the mesozoic lithospheric mantle and tectonic decoupling beneath the Dabie Orogen, central China: Evidence from $^{40}\text{Ar}/^{39}\text{Ar}$ geochronology, elemental and Sr-Nd-Pb isotopic compositions of early Cretaceous mafic igneous rocks. *Chemical Geology*, 220: 165–189.
- Wu Hui, Zhang Yinghua, Ling Wenli, Bai Xiao, Ma Qian, Berkana, W., Cheng Jianping and Peng Lianhong, 2016. Recognition of mantle input and its tectonic implication for the nature of –815 Ma magmatism in the Yangtze continental interior, South China. *Precambrian Research*, 279: 17–36.
- Xu Haijin, Ma Changqian, Song Yanru, Zhang Junfeng and Ye Kai, 2012. Early Cretaceous intermediate-mafic dykes in the Dabie Orogen, eastern China: Petrogenesis and implications for crust-mantle interaction. *Lithos*, 154: 83–99.
- Yang Fuquan, Liu Feng, Li Qiang and Geng Xinxia, 2014. In situ LA-MC-ICP-MS U-Pb geochronology of igneous rocks in the Ashele Basin, Altay orogenic belt, northwest China: Constraints on the timing of polymetallic copper mineralization. *Journal of Asian Earth Sciences*, 79: 477–496.
- Yao Jinlong, Shu Liangshu, Santosh, M., and Li Jinyi, 2013. Geochronology and Hf isotope of detrital zircons from Precambrian sequences in the eastern Jiangnan Orogen: Constraining the assembly of Yangtze and Cathaysia blocks in South China. *Journal of Asian Earth Sciences*, 74: 225–243.
- Yao, Jinlong., Shu, Liangshu., Santosh, M., and Li, Jinyi., 2015. Neoproterozoic arc-related andesite and orogeny-related unconformity in the eastern Jiangnan orogenic belt: Constraints on the assembly of the Yangtze and Cathaysia blocks in South China. *Precambrian Research*, 262: 84–100.
- Yin Jiuyan, Chen Wen, Xiao Wenjiao, Yuan Chao, Windley, B.F., Yu Shun and Cai Keda, 2017. Late Silurian–early

- Devonian adakitic granodiorite, A-type and I-type granites in NW Junggar, NW China: Partial melting of mafic lower crust and implications for slab roll-back. *Gondwana Research*, 43: 55–73.
- Yin Jiyuan, Chen Wen, Xiao Wenjiao, Yuan Chao, Zhang Bin, Cai Keda and Long Xiaoping, In press. Geochronology, petrogenesis, and tectonic significance of the latest Devonian-early Carboniferous I-type granites in the Central Tianshan, NW China. *Gondwana Research*.
- Yuan Shunda, Peng Jiantang, Hao Shuang, Li Huimin, Geng Jianzhen and Zhang Dongliang, 2011. In situ LA-MC-ICP-MS and ID-TIMS U–Pb geochronology of cassiterite in the giant Furong tin deposit, Hunan Province, South China: New constraints on the timing of tin–polymetallic mineralization. *Ore Geology Reviews*, 43: 235–242.
- Zhang Heng, Li Tingdong, Xie Ying, Zhang Chuanheng, Gao Linzhi, Geng Shufang, Chen Tingyu and You Guoqing, 2015. Geochronology and Tectonic Evolution of the West Section of the Jiangnan Orogenic Belt. *Acta Geologica Sinica* (English Edition), 89(5): 1497–1515.
- Zhang Yuzhi, Wang Yuejun, Zhang Yanhua and Zhang Aimei, 2015. Neoproterozoic assembly of the Yangtze and Cathaysia blocks: Evidence from the Cangshuipu Group and associated rocks along the central Jiangnan Orogen, South China. *Precambrian Research*, 269: 18–30.
- Zhao Guochun, 2015. Jiangnan Orogen in South China: Developing from divergent double subduction. *Gondwana Research*, 27: 1173–1180.
- Zhao Junhong, 2008. *Geochemistry of Neoproterozoic arc-related plutons in the western margin of the Yangtze Block, South China*. Hongkong: The University of Hongkong (Ph. D thesis): 1–315.
- Zhao Junhong, Zhou Meifu, Yan Danping, Yang Yueheng and Sun Min, 2008. Zircon Lu–Hf isotopic constraints on Neoproterozoic subduction-related crustal growth along the western margin of the Yangtze Block, South China. *Precambrian Research*, 163: 189–209.
- Zhao Junhong, Zhou Meifu, Yan Danping, Zheng Jianping and Li Jianwei, 2011. Reappraisal of the ages of Neoproterozoic strata in South China: No connection with the Grenvillian orogeny. *Geology*, 39: 299–302.
- Zhao Xinfu, 2010. *Paleoproterozoic crustal evolution and Fe-Cu metallogeny of the western Yangtze Block, SW China*. Hongkong: The University of Hongkong (Ph. D thesis): 1–179.
- Zheng Yongfei, Wu Rongxin, Wu Yuanbao, Zhang Shaobing, and Yuan Honglin, 2008. Rift melting of juvenile arc-derived crust: Geochemical evidence from Neoproterozoic volcanic and granitic rocks in the Jiangnan Orogen, South China. *Precambrian Research*, 163: 351–383.
- Zheng Yongfei, Zhang Shaobing, Zhao Zifu, Wu Yuanbao, Li Xianhua, Li Zhengxiang and Wu Fuyuan, 2007. Contrasting zircon Hf and O isotopes in the two episodes of Neoproterozoic granitoids in South China: Implications for growth and reworking of continental crust. *Lithos*, 96: 127–150.
- Zhou Meifu, Ma Yuxiao, Yan Danping, Xia Xiaoping, Zhao Junhong and Sun Min, 2006. The Yanbian Terrane (southern Sichuan Province, SW China): A Neoproterozoic arc assemblage in the western margin of the Yangtze Block. *Precambrian Research*, 144: 19–38.
- Zhou Meifu, Yan Danping, Kennedy, A.K., Li Yunqian and Ding Jun, 2002. SHRIMP U–Pb zircon geochronological and geochemical evidence for Neoproterozoic arc-magmatism along the western margin of the Yangtze Block, South China. *Earth and Planetary Science Letters*, 196: 51–67.
- Zhou Meifu, Zhao Junhong, Xia Xiaoping, Sun Weihua and Yan Danping, 2007. Comment on “Revisiting the “Yanbian Terrane”: Implications for Neoproterozoic tectonic evolution of the western Yangtze Block, South China” [Precambrian Res. 151 (2006) 14–30]. *Precambrian Research*, 155: 313–317.

About the first author

MABI Awei, male, A PhD candidate from the School of Earth Sciences, Chengdu University of Technology. He majors in geology and his field of study is petrology and geochemistry of igneous rocks. His previous works focused on the magmatism and tectonic evolution of the eastern Tethys, as well as the granite, ophiolite, volcanic rocks in the Central Asian Orogenic Belt. Now his research interests focus on the Precambrian magmatic-tectonic events in the western Yangtze Block, south western China. Email: 406305000@qq.com; Phone: (+86)13028144884.